Secrecy Rate of Cooperative MIMO in Presence of a Location Constrained Eavesdropper

Zhong Zheng, *Member, IEEE,* Zygmunt J. Haas, *Fellow, IEEE*, and Mario Kieburg[1]

Abstract

We propose and study the secrecy cooperative MIMO architecture to enable and to improve the secrecy transmissions between clusters of mobile devices in presence of an eavesdropper with certain location constraint. The cooperative MIMO is formed by temporarily activating clusters of nearby trusted devices, with each cluster being centrally coordinated by its corresponding cluster head. We assume that the transmitters apply a practical eigen-direction precoding scheme and that the eavesdropper has multiple possible locations in the proximity of the legitimate devices. We first obtain the expression of the secrecy rate, where the required average mutual information between the transmit cluster and the eavesdropper is characterized by closed-form approximations. The proposed approximations are especially useful in the secrecy rate maximization, where the original non-convex problem is approximated by a sequence of convex sub-problems. Numerical results show that the achievable secrecy rate can be effectively improved by activating equal or larger number of trusted devices as compared to the number of antennas at the eavesdropper. The secrecy rate is further improved by increasing the cluster size.

Index Terms

Cooperative MIMO; RD-MIMO; mobile networks; physical-layer security; random matrix theory.

Z. Zheng was with the Department of Computer Science, University of Texas at Dallas, Richardson, TX 75080 USA (e-mail: zhong.zheng.z@ieee.org).

Z. J. Haas is with the Department of Computer Science, University of Texas at Dallas, Richardson, TX 75080 USA, and also with the School of Electrical and Computer Engineering, Cornell University, Ithaca, NY 14853 USA (e-mail: zhaas@cornell.edu).

M. Kieburg is with the Faculty of Physics, Bielefeld University, PO-Box 100131, 33501 Bielefeld, Germany (e-mail: mkieburg@physik.uni-bielefeld.de).

I. INTRODUCTION

The physical-layer security has recently attracted increasing attention in the field of wireless communications, as it guarantees information security between the legitimate entities even when the eavesdropper overhears the communications [1]. Unlike the conventional cryptographic methods, the physical-layer security does not rely on key-based encryption for the confidential message. Instead, the legitimate transmitter utilizes the characteristics of the communication channels to encode the information such that the confidential message is conveyed to the legitimate receiver, while the information leakage to the eavesdropper is eliminated in the information-theoretical sense [2]. Therefore, the physical-layer security guarantees perfect information secrecy between legitimate transceivers and circumvents the challenges in the conventional key-based encryption, such as key distribution and management, which are especially critical in wireless communication due to its broadcasting nature.

Throughout this paper, we refer to the legitimate transmitter(s) and the legitimate receiver(s) as Alice and Bob, respectively, and refer to the eavesdropper as Eve. Under the secrecy constraint, the maximum information rate between Alice and Bob is characterized by the secrecy capacity. As shown in [2] and [3], the secrecy capacity is the difference between the Shannon rates of the legitimate channel between Alice and Bob and the eavesdropping channel between Alice and Eve, under the condition that the mutual information between Alice and Eve is zero. Therefore, a positive secrecy rate amounts to having channel advantage between Alice and Bob. When Alice, Bob, and Eve are all equipped with a single antenna, obtaining a positive secrecy rate requires the Signal-to-Noise Ratio (SNR) received at Bob to be strictly larger than the received SNR at Eve. Under the fading channels, authors in [4] consider the ergodic secrecy capacity, where a positive ergodic secrecy rate can still be achieved even when the average SNR received at Bob is worse than the average SNR at Eve.

Multi-antenna transceivers increase the spatial degrees of freedom of the end-to-end channel, which can be leveraged to improve the secrecy rate [5]. When Alice has a single antenna and Bob has multiple antennas, a.k.a. the Single-Input Multi-Output (SIMO) wiretap channel, the secrecy capacity and the outage secrecy capacity were investigated in [6] and [7], while the corresponding MISO case was studied in [8] and [9]. The secrecy capacity of a special case of the MIMO wiretap

channel was considered in [10], where Alice and Bob are equipped with dual antennas, and Eve is equipped with a single antenna. Recently, the physical-layer security has also been considered for the Distributed-MIMO (D-MIMO) systems in [11]–[15], where Alice has a distributed antenna array composed of remote antenna ports or base stations. Therein, the distributed antenna elements are connected to the central base station via tethered high-speed fiber links, and the considered D-MIMO systems are relevant for the infrastructure cellular communication systems. The D-MIMO configurations further improve the secrecy capacity by leveraging the macro diversity due to more diverse path losses and shadowing [12]. In addition, as the distributed antenna elements are typically separated by a larger distance compared to the wavelength, some of the harmful propagation effects, such as the spatial correlation [16] and the double-scattering fading [17], can be eliminated. Unlike the infrastructure D-MIMO systems, the proposed cooperative MIMO architecture is based on forming the distributed antenna arrays on-demand, where each array is composed of a cluster of nearby legitimate mobile devices. The cooperative MIMO improves the secrecy rate between the clusters by leveraging the benefits of distributed MIMO, while having the flexibility in the topology and the size of the formed antenna arrays.

A. Related Works

Evaluating the secrecy capacity amounts to finding the optimal transmitted signals of Alice, which maximizes the difference between the mutual information of the legitimate and the eavesdropping channels. In the MIMO wiretap channels, the problem becomes optimizing the input covariance matrix, which is a difficult non-convex problem. Previous works showed that the design of the optimal input heavily depends on the antenna configurations of the MIMO channels and the amount of Channel State Information at Transmitter (CSIT) available at Alice. In particular, when both Alice and Eve are equipped with multiple antennas, Bob has a single antenna, and Alice has CSITs of both channels, authors in [18] show that the capacity-achieving transmitter scheme is beamforming. The beamforming direction is chosen as the generalized eigenvector corresponding to the maximum generalized eigenvalue of the wiretap channel. When Bob is also equipped with multiple antennas, the conditions of a full rank and a rank deficient input covariance matrix are proved in [19]. In [20] and [21], the structures of the optimal input covariance matrix are characterized for general multi-antenna wiretap channels. The closed-form expression of the

optimal input is given in [22] when the input covariance matrix is full rank, and is given in [23] when it is either full rank or of rank-one.

In the context of secrecy communications, the eavesdropper is usually passive and silent. Therefore, it is more practical to assume only the statistical, rather than the full knowledge, of the CSIT of the eavesdropping channel. Compared to the full CSIT counterpart, there is much fewer result available for the secrecy capacity under the statistical CSIT assumption. The optimal transmitter can be only characterized for certain channel configurations. When Alice has multiple antennas, and both Bob and Eve have single receive antenna, [24] provides a sufficient condition for the optimal input covariance matrix being rank-one. In the same setting, authors in [25] derive the closed-form expressions for the optimal input covariance matrix, where the artificial noise is injected and optimized. The optimal rank-one input covariance matrix has been also identified in [26] when Eve is equipped with multiple receive antennas, and an on-off power allocation scheme is proposed in [27] to maximize the secrecy rate. When the statistical CSITs of both channels are available and Bob has more receive antennas compared to Eve, authors in [28] show that the optimal input covariance matrix is an identity matrix with uniform power allocation across the transmit antennas. However, when the instantaneous CSIT of the legitimate channel and the statistical CSIT of the eavesdropping channel are available, the capacity-achieving transmitter design is still unknown for generic antenna configurations.

Alternatively, the secrecy rate maximization, assuming statistical CSIT of the eavesdropping channel, has been pursued by approximating the information rate between Alice and Eve, which leads to a simplified optimization problem. In [29], the average mutual information between Alice and Eve is upper-bounded by a deterministic channel and the optimal precoding has the same direction as the generalized eigenvector of the approximate wiretap channels. In [30], the average mutual information is lower-bounded with a simplified analytical expression and the upper bound of secrecy rate is obtained by assuming linear precoding at the transmitter. By approximating the average rate of Eve with its Taylor series expansion, the non-convex secrecy rate maximization reduces to a sequence of convex sub-problems [31]. In [12], assuming multiple distributed transmitters, the secrecy rate maximization is converted to a max-min problem using results from the Random Matrix Theory and solved by the iterative block coordinate descent algorithm. However, the techniques used in [12] and [29]–[31] are relevant to the MIMO channels with co-

located antenna arrays or a single distributed antenna array, and cannot be applied to the MIMO channels with distributed antennas at both Alice and Bob, as we assumed in this paper.

B. *Physical-Layer Security of Cooperative MIMO*

In our recent work [32], we studied a mobile cooperative MIMO architecture, which is also termed as the Reconfigurable Distributed MIMO (RD-MIMO). Therein, a group of nearby mobile nodes forms a node cluster to jointly transmit or receive wireless signals. The cluster is coordinated by a head node and the coordination signaling is exchanged within the cluster via local wireless connections. When two clusters communicate with each other, and the head node of each cluster jointly encodes or decodes the communicated symbols, the distributed antenna arrays resemble the D-MIMO system. In this work, we consider the physical-layer security of the communications between two clusters of legitimate nodes, each collectively called Alice and Bob, respectively. The inter-cluster transmissions are wiretapped by an eavesdropper, which may be placed at some possible locations near the legitimate devices. As will be discussed in the following sections, the cooperative MIMO framework improves the secrecy rate both effectively and flexibly. On the one hand, compared to the secured transmissions between two single devices, the spatial degrees of freedom between the clusters are increased, which can be utilized in designing the secrecy transmission. On the other hand, the node cluster can be formed on-demand and the number of nodes in the cluster can be determined according to the needed performance requirement.

We summarize the contributions of applying the physical-layer security in the cooperative MIMO framework:

- We assume Eve may appear at a finite but arbitrary number of possible locations. The eavesdropper keeps silent and Alice only has the statistical CSITs of the eavesdropper's channels corresponding to each of the possible locations[2]. This system model can be used to evaluate the achievable secrecy rate of the cooperative MIMO, where the locations of

---

[2] In order to fulfill certain location constraint, Eve should be located within a continuous region or on a continuous contour. However, as will be shown in Section IV, the region or the contour constraint can be well-approximated by placing Eve on a sufficiently large number of discrete possible locations. We will leave the study of a region-constrained Eve in future work.

Eve are loosely constrained without specifying a known location. For example, Eve may be separated from Alice with a certain minimum distance.

- We consider eigen-direction precoding ([9]) to construct the input covariance matrix, which reduces the original problem to a lower dimensional power allocation problem. Accordingly, we derive approximations for the average rate between Alice and Eve as a function of the power allocation vector. Numerical results show that the proposed approximations are reasonably accurate and provide over-estimates for the exact average rate with a large probability. This is relevant in the context of physical-layer security to fulfill the secrecy constraint. In addition, compared to the exact expression of the average rate between Alice and Eve, the proposed approximations are explicit functions of the power allocation vector. This is a useful property to further approximate the average rate, a concave function of the power allocation vector, with a linear affine function, which greatly simplifies the secrecy rate maximization.

- The non-convex secrecy rate maximization, assuming a number of possible locations of Eve, is converted into a sequence of convex sub-problems using the affine approximations for the average rate between Alice and Eve. Each sub-problem can be efficiently solved by standard convex optimization tools. Numerical results show that by enabling more legitimate nodes to form the cooperative clusters, significant secrecy rate can be achieved even when Eve is closer to Alice. On the other hand, when Eve has more receive antennas compared to Alice and Bob, using a more dispersive node distribution can eliminate the outage of secrecy transmissions.

The rest of the paper is organized as follows: Section II introduces the signal model of cooperative MIMO wiretap channels and outlines the eigen-direction precoding scheme. In Section III, we derive approximations for the average rate between Alice and Eve using the eigen-direction precoding. Numerical results are illustrated to validate the accuracy of the proposed approximations. In Section IV, we present the secrecy rate maximization framework and the related numerical results. In Section V, we conclude the findings of this paper.

II. SYSTEM MODEL

Consider a pair of legitimate transmit and receive nodes, which are hereafter referred to as the
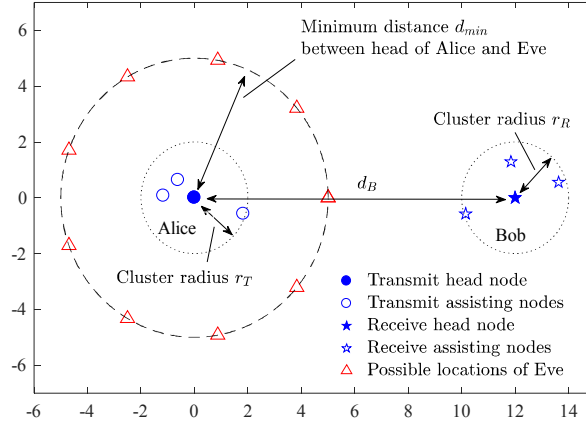
Fig. 1. Cooperative MIMO in presence of an eavesdropper. The possible locations of the eavesdropper have a minimum distance $d_{\min}$ towards the head of Alice. The distance between head nodes of Alice and Bob is d_B.

transmit and receive head nodes. The confidential information is transmitted between the head nodes over the wireless channel and prone to be eavesdropped by a malicious listener, as shown in Fig. 1. In the circular area centering at the transmit head node with radius r_T, we assume there is a cluster with $K-1$ trusted transmit nodes and the transmit cluster is collectively referred to as Alice. Similarly, in the circular area centering at the receive head node with radius r_R, there are $N-1$ trusted receive nodes and the receive cluster is collectively referred to as Bob. All the legitimate and trusted nodes are equipped with a single antenna, while the malicious listener is equipped with an M-antenna array. In typical communication systems, the eavesdropper is silent and the legitimate nodes cannot detect its presence. However, in certain scenarios, it is relevant to assume that the locations of the eavesdropper are constrained to possible locations, and that the communication between the legitimate nodes can be configured according to the prior knowledge of such possible locations. As an example, Fig. 1 shows the possible locations of the eavesdropper, when a minimum distance $d_{\min}$ is imposed between the transmit head node and the eavesdropper.

Using the RD-MIMO framework as discussed in [32], the K transmit nodes forms a cooperative transmit cluster, where the head node is responsible for encoding the information symbols into transmit signals, distributes the encoded signals to the cluster nodes, and synchronizes the transmissions within the cluster. Similarly, the N receive nodes form the

cooperative receive cluster, in which the receive head node collects the received signals from its assisting nodes and jointly decodes the receive symbols. We assume the node cooperation within each cluster is performed over high-speed wireless connections, while the transmissions between clusters have much lower rate due to longer distance and more severe channel impairments. Therefore, the inter-cluster transmissions are the bottleneck of the system, and the channels between Alice and Bob resemble the D-MIMO channels. In addition, we focus on the physical layer security of the inter-cluster communication, where the communication between Alice and Bob in presence of Eve is modeled by the MIMO wiretap channel [20]. We assume the security of the intra-cluster communication within Alice and Bob can be guaranteed relatively easily, because the communication links have shorter range and have higher channel capacity.

A. Signal Model

Given a transmit vector $\mathbf{x} = [x_1, \dots, x_K]^{\mathrm{T}}$, where x_k denotes the transmit signal of the kth transmit node in Alice, the vector $\mathbf{y} = [y_1, \dots, y_N]^{\mathrm{T}}$ denotes the receive signals at Bob, and $\mathbf{z}_i = [z_{i,1}, \dots, z_{i,M}]^{\mathrm{T}}$, $i = 1, \dots, L$, denotes the receive signals at Eve when Eve is at the ith location:

$$\mathbf{y} = \sqrt{g_B}\mathbf{H}\mathbf{x} + \mathbf{n}_B, \tag{1}$$

$$\mathbf{z}_i = \sqrt{g_E}\mathbf{F}_i\mathbf{x} + \mathbf{n}_E, \tag{2}$$

where L is the number of possible locations of Eve, y_n and $z_{i,m}$ are the receive signal of the nth node at Bob ($1 \leq n \leq N$) and of the mth antenna at Eve ($1 \leq m \leq M$), respectively. The MIMO channel between Alice and Bob is denoted as $\mathbf{H}$, where the entry $\mathbf{H}_{n,k}$ is the channel coefficient between the kth transmit node in Alice and the nth receive node in Bob. The channel coefficient $\mathbf{H}_{n,k}$ is modeled as the complex Gaussian random variable with zero mean and variance $\beta_{n,k}$, where $\beta_{n,k}$ is the normalized average channel gain given by

$$\beta_{n,k} = \frac{\mathrm{PL}(d_{n,k})}{g_B} = \left(\frac{d_B}{d_{n,k}}\right)^{\alpha}. \tag{3}$$

Here, $\alpha(\geq 2)$ is the path-loss exponent, $\mathrm{PL}(d) = c_p d^{-\alpha}$ is the average channel gain between two nodes at a distance d, c_p is the path loss at the unit distance, and $g_B = \mathrm{PL}(d_B)$ denotes the average channel gain between the head nodes of Alice and Bob.

The channel coefficients between Alice and Eve are denoted as $\mathbf{F}_i = \mathbf{W}_i\boldsymbol{\Sigma}_i^{1/2}$, where the

$M \times K$ matrix $\mathbf{W}_i$ denotes the fast fading coefficients, modeled by *i.i.d.* standard complex Gaussian random variables. The $K \times K$ diagonal matrix $\boldsymbol{\Sigma}_i$ denotes the average channel gains between Alice and Eve with the kth diagonal entry $\sigma_{i,k}$ being

$$\sigma_{i,k} = \frac{\mathrm{PL}(d_{i,k})}{g_E} = \left(\frac{d_E}{d_{i,k}}\right)^{\alpha}, \tag{4}$$

where $d_{i,k}$ is the distance between the kth node of Alice and the ith location of Eve, and $g_E = \mathrm{PL}(d_E)$ denotes the average channel gain between the head node of Alice and Eve. The additive noise $\mathbf{n}_B$ at Bob and $\mathbf{n}_E$ at Eve are modeled as *i.i.d.* complex Gaussian vectors with powers N_0, i.e., $\mathbf{n}_B \sim \mathcal{CN}(\mathbf{0}, N_0 \mathbf{I}_N)$ and $\mathbf{n}_E \sim \mathcal{CN}(\mathbf{0}, N_0 \mathbf{I}_M)$.

In this work, we adopt the following signal-level assumptions:

1. The channels $\mathbf{H}$ and $\mathbf{F}_i$ are frequency flat and follow the block fading process, i.e., the entries of $\mathbf{H}$ and $\mathbf{F}_i$ vary independently from one channel coherent time to another, but remain constant for each coherent time.

2. The instantaneous CSI of $\mathbf{H}$ is known by the nodes in Alice, Bob, and Eve. The instantaneous CSI $\mathbf{F}_i$ is only known by Eve, while the statistical CSIs of $\mathbf{F}_i$, $i = 1, \ldots, L$, are available to Alice.

The statistical CSI of $\mathbf{F}_i$ relies on the distance-dependent path loss and the number of available antennas at Eve, which is acquired from prior knowledge. For example, there may exist a maximum number of antenna $M_{\max}$ that Eve can be equipped with and a minimum distance $d_{\min}$ between the head node of Alice and Eve. By setting $M = M_{\max}$ and $d_E = d_{\min}$, a lower bound of the secrecy rate can be evaluated. The achievable secrecy rate and a practical precoding scheme are discussed in the next subsection.

B. Secrecy Rate and Precoder Design

The considered wiretap channel model with multiple possible locations of Eve is equivalent to the compound wiretap channel with the receiver CSI [33]. In particular, denote the channel input as $\mathcal{X}$, the channel output at the legitimate receiver as $\mathcal{Y}$, and the output at the ith eavesdropper as $\mathcal{Z}_i$, $1 \leq i \leq L$. According to [33, Prop. 6], the following secrecy rate $\widehat{R}_{\mathrm{sec}}$ is achievable

$$\widehat{R}_{\mathrm{sec}} = \max_{p(\mathcal{V}, \mathcal{X})} \left[I(\mathcal{V}; \mathcal{Y}) - \max_{1 \leq i \leq L} I(\mathcal{V}; \mathcal{Z}_i) \right]^+, \tag{5}$$

where $[x]^+ = \max(0, x)$, $I(a; b)$ denotes the mutual information between the random variables a and b, $\mathcal{V}$ is an auxiliary random variable, and $\mathcal{V} \to \mathcal{X} \to (\mathcal{Y}, \mathcal{Z}_i)$, $1 \leq i \leq L$, form the Markov chains. The outer maximization in (5) is optimized over the joint distribution $p(\mathcal{V}, \mathcal{X})$ of the random variables $\mathcal{V}$ and $\mathcal{X}$. Since the CSIs are available to the receivers, the outputs of the compound channel at the eavesdroppers can be viewed as the tuples $\mathcal{Z}_i = \{\mathbf{z}_i, \mathbf{F}_i\}$. By using the chain rule of mutual information, we obtain

$$I(\mathcal{V}; \mathcal{Z}_i) = I(\mathcal{V}; \mathbf{z}_i, \mathbf{F}_i) = I(\mathcal{V}; \mathbf{z}_i | \mathbf{F}_i) + I(\mathcal{V}; \mathbf{F}_i) = I(\mathcal{V}; \mathbf{z}_i | \mathbf{F}_i), \tag{6}$$

where $I(\mathcal{V}; \mathbf{F}_i) = 0$ since the instantaneous channel is unknown to the transmitter and therefore $\mathcal{V}$ and $\mathbf{F}_i$ are independent. Similarly, $I(\mathcal{V}; \mathcal{Y}) = I(\mathcal{V}; \mathbf{y}, \mathbf{H})$ by treating $\mathcal{Y} = \{\mathbf{y}, \mathbf{H}\}$.

By setting $\mathcal{V} = \mathbf{x}$ and assuming Gaussian signaling at the transmitter, i.e., $\mathbf{x} \sim \mathcal{CN}(\mathbf{0}, \mathbf{Q})$ with $\mathbf{Q} \succ \mathbf{0}$ a positive definite Hermitian matrix, a lower bound of the secrecy rate $\widehat{R}_{\mathrm{sec}}$ can be obtained. In specific, $I(\mathbf{x}; \mathbf{y}, \mathbf{H})$ and $I(\mathbf{x}; \mathbf{z}_i | \mathbf{F}_i)$ are the well-known mutual information of the Gaussian MIMO channels [34], and a lower bound of $\widehat{R}_{\mathrm{sec}}$ can be explicitly written as

$$\max_{\mathbf{0} \prec \mathbf{Q}} \left[\log \det \left(\mathbf{I} + \tfrac{g_B}{N_0} \mathbf{H} \mathbf{Q} \mathbf{H}^\dagger \right) - \max_{1 \leq i \leq L} \mathbb{E} \left[\log \det \left(\mathbf{I} + \tfrac{g_E}{N_0} \mathbf{F}_i \mathbf{Q} \mathbf{F}_i^\dagger \right) \right] \right]^+, \text{ s.t. } 0 \leq \mathrm{tr}(\mathbf{Q}) \leq P, \tag{7}$$

where P denotes the total maximum transmit power. According to the definition of the conditional mutual information, the expectation in (7) is taken over the distribution of $\mathbf{F}_i$. Although the Gaussian signaling may be sub-optimal for generic wiretap channels, it is widely adopted due to its tractability, e.g. see [7]-[15], [18]-[28].

The secrecy rate (7) requires optimizing over the Hermitian covariance matrix $\mathbf{Q}$, which involves a parametric space with K^2 degrees of freedom. To reduce the optimization complexity and simplify the transceiver design, we adopt the eigen-direction precoding [9], where the covariance matrix $\mathbf{Q}$ is constructed by the eigenvectors of the main channel $\mathbf{H}$ and a K-dimensional power allocation vector, so as to reduce the dimension of the parametric space to K. Specifically, by using the singular value decomposition, the channel $\mathbf{H}$ can be rewritten as

$$\mathbf{H} = \mathbf{V}_0 \mathbf{\Lambda}^{1/2} \mathbf{V}_1^\dagger, \tag{8}$$

where the $N \times N$ matrix $\mathbf{V}_0$ and the $K \times K$ matrix $\mathbf{V}_1$ are unitary, and $\mathbf{\Lambda}$ is an $N \times K$ rectangular diagonal matrix with the diagonal entries $\mathbf{\Lambda}_{k,k} = \lambda_k$, $1 \leq k \leq \min(K, N)$, being the non-zero eigenvalues of $\mathbf{H} \mathbf{H}^\dagger$. The transmitted signal $\mathbf{x}$ is constructed by the matrix $\mathbf{V}_1$ and a

diagonal matrix $\mathbf{\Psi}$, such that

$$\mathbf{x} = \sqrt{P}\mathbf{V}_1\mathbf{\Psi}^{1/2}\mathbf{s}, \tag{9}$$

where $\mathbf{s} \in \mathbb{C}^{K\times 1}$ are the transmit symbols with normalized power, i.e., $\mathbb{E}[\mathbf{ss}^\dagger] = \mathbf{I}$. The kth diagonal entry of $\mathbf{\Psi}$, ψ_k, denotes the fraction of total power allocated to the kth transmit symbol and satisfies $0 \leq \mathrm{tr}(\mathbf{\Psi}) \leq 1$. Denote $\gamma_B = Pg_B/N_0$ and $\gamma_E = Pg_E/N_0$ as the average SNR received by Bob and Eve, respectively, and denote $\gamma_k = \gamma_E\psi_k$, $1 \leq k \leq K$. Using the eigen-direction precoder (9), i.e. setting $\mathbf{Q} = P\mathbf{V}_1\mathbf{\Psi}\mathbf{V}_1^\dagger$, the secrecy rate (7) is further lower-bounded and is written in terms of $\boldsymbol{\gamma} = [\gamma_1, \ldots, \gamma_K]^\mathrm{T}$ as

$$R_{\mathrm{sec}} = \max_{\boldsymbol{\gamma}\in\mathcal{P}}[R_s(\boldsymbol{\gamma})]^+, \quad \text{s.t. } \textstyle\sum_{i=1}^K \gamma_i \leq \gamma_E, \tag{10}$$

where $\mathcal{P} = \{\gamma_i \geq 0, 1 \leq i \leq K\}$ denotes the space of K-dimensional non-negative vectors. The function $R_s(\boldsymbol{\gamma})$ is given by

$$R_s(\boldsymbol{\gamma}) = \textstyle\sum_{i=1}^K \log\left(1 + \frac{\gamma_B}{\gamma_E}\bar{\lambda}_i\gamma_i\right) - \max_{1\leq i\leq L}\overline{R}_{E,i}(\boldsymbol{\gamma}), \tag{11}$$

where $\bar{\lambda}_i = \lambda_i$ for $1 \leq i \leq \min(N, K)$ and $\bar{\lambda}_i = 0$ otherwise. The rate $\overline{R}_{E,i}(\boldsymbol{\gamma})$ is written as

$$\overline{R}_{E,i}(\boldsymbol{\gamma}) = \mathbb{E}\left[\log\det\left(\mathbf{I} + \mathbf{W}_i\mathbf{\Sigma}_i^{1/2}\mathbf{V}_1\mathbf{\Gamma}\mathbf{V}_1^\dagger\mathbf{\Sigma}_i^{1/2}\mathbf{W}_i^\dagger\right)\right], \tag{12}$$

where $\mathbf{\Gamma}$ is a $K \times K$ diagonal matrix with the ith diagonal entry being γ_i. Note that $\overline{R}_{E,i}(\boldsymbol{\gamma})$ depends on the channel $\mathbf{H}$ via the precoding matrix $\mathbf{V}_1$, which is fixed under the expectation operation. We will derive in Section III the approximations for the average rate $\overline{R}_{E,i}(\boldsymbol{\gamma})$ under different channel settings, and present an optimization framework in Section IV to obtain the optimal power allocation to maximize R_{sec} in (10).

Although the precoding structure (9) is heuristic and is generally not optimal due to the reduction in the degrees of freedom, it is a reasonable scheme and leads to low-complexity transceiver design. First, we note that under the same channel knowledge assumption, the eigen-direction precoding achieves global optimal when Bob and Eve are equipped with single antenna [24], and has been also adopted in other multi-antenna communication systems such as in [9] and [34]. Second, by multiplying the receive signal $\mathbf{y}$ with the unitary matrix $\mathbf{V}_0^\dagger$, the received signals are decomposed into orthogonal parallel data streams with amplitudes proportional to λ_k, $1 \leq k \leq \min(K, N)$, and therefore, simplifying the receiver design.

III.   AVERAGE RATE OF EIGEN-DIRECTION PRECODING

In this section, we present analytical approximations for the average rate $\overline{R}_{E,i}(\boldsymbol{\gamma})$ between Alice and Eve, given a certain power allocation vector $\boldsymbol{\gamma}$. Compared to the exact expression for the average rate $\overline{R}_{E,i}(\boldsymbol{\gamma})$, the proposed approximations are explicit functions of the optimizing variable $\boldsymbol{\gamma}$, which can be conveniently used to deduce the linear affine approximation for the average rate. As will be shown in Section IV, the affine approximation of $\overline{R}_{E,i}(\boldsymbol{\gamma})$ is the key ingredient to convert the non-convex problem (10) into a sequence of simple convex sub-problems. Under some typical system settings of the cooperative MIMO, we also present examples of numerical results to illustrate the approximation error incurred by using the proposed approximations. For notational simplicity, we drop the dependency on the power allocation vector $\boldsymbol{\gamma}$ and the location index i from the average rate $\overline{R}_{E,i}(\boldsymbol{\gamma})$ and its approximation, whenever it is clear from the context.

A. Average Rate Between Alice and Eve

Given a certain power allocation vector $\boldsymbol{\gamma}$, the average rate $\overline{R}_E$ in (12) has the same formulation as the correlated Rayleigh MIMO channel with the transmitter-side correlation, which is available in literature [36]. However, by using the expression [36, Eq. (123)], the average rate $\overline{R}_E$ depends on the power allocation $\boldsymbol{\gamma}$ via the eigenvalues of $\boldsymbol{\Sigma}^{1/2}\mathbf{V}_1\boldsymbol{\Gamma}\mathbf{V}_1^{\dagger}\boldsymbol{\Sigma}^{1/2}$, instead of $\boldsymbol{\gamma}$ itself. As a result, it is inconvenient to use $\overline{R}_E$ to search for the optimal power allocation, as it incurs prohibitively large computation demands to solve the eigenvalue problems. In addition, the implicit function $\overline{R}_E$ prevents further manipulations to simplify the secrecy rate optimization procedures, such as those described in Section IV.

To address this issue, we propose approximations for the average rate $\overline{R}_E$, which will directly depend on the power allocation vector $\boldsymbol{\gamma}$. In specific, consider the quantity $\bar{\mathcal{Q}}_E(\boldsymbol{\gamma})$ constructed as follows:

$$\bar{\mathcal{Q}}_E(\boldsymbol{\gamma}) = \log \mathbb{E}\big[\det(\mathbf{I} + \mathbf{W}\boldsymbol{\Sigma}^{1/2}\mathbf{U}\boldsymbol{\Gamma}\mathbf{U}^{\dagger}\boldsymbol{\Sigma}^{1/2}\mathbf{W}^{\dagger})\big], \qquad (13)$$

where the expectation is taken over both $\mathbf{W}$ and the Haar random unitary matrix $\mathbf{U} \in \mathcal{U}(K)$. We denote $\mathcal{U}(K)$ as the unitary group containing all $K \times K$ unitary matrices [37]. Comparing

(13) with (12), we replace the fixed unitary matrix $\mathbf{V}_1$ with the random unitary matrix $\mathbf{U}$ and apply the Jensen's inequality for the concave $\log\det$ function. Intuitively, when the path-loss matrix $\mathbf{\Sigma}$ is close to an identity matrix, the unitary matrix $\mathbf{V}_1$ or $\mathbf{U}$ commutes with $\mathbf{\Sigma}$ and can be absorbed into the unitary invariant matrix $\mathbf{W}$. The quantity $\bar{\mathcal{Q}}_E$ then becomes the strict upper bound of the average rate $\overline{R}_E$. We will also show in the numerical results that $\bar{\mathcal{Q}}_E$ can serve as an accurate approximation for $\overline{R}_E$, under typical settings of the cooperative MIMO systems.

In the following, we will denote $\{\mathcal{M}_{i,j}\}_{1\leq i\leq a, 1\leq j\leq b}$ as an $a \times b$ matrix block, where the row and column indices run from 1 to a and from 1 to b, respectively. We denote $\Delta_m(\boldsymbol{a}) = \det[a_i^{j-1}] = \prod_{1\leq j<k\leq m}(a_k - a_j)$ as the Vandermonde determinant and denote $_pF_q\left(\begin{array}{c}a_1,\ldots a_p\\b_1,\ldots b_q\end{array}\middle| x\right)$ as the generalized hypergeometric function with $p+q$ parameters [37, Eq. (9.14.1)]. When $|x| < 1$, it admits the series representation,

$$_pF_q\left(\begin{array}{c}a_1,\ldots a_p\\b_1,\ldots b_q\end{array}\middle| x\right) = \sum_{n=0}^{\infty} \frac{(a_1)_n\cdots(a_p)_n}{(b_1)_n\cdots(b_q)_n}\frac{x^n}{n!}, \tag{14}$$

where $(a)_n = \Gamma(a+n)/\Gamma(a)$ is the Pochhammer symbol.

In the following propositions, without loss of generality, we present the expressions of $\bar{\mathcal{Q}}_E$ when the power allocation variables are ordered, i.e., $\gamma_1 \geq \cdots \geq \gamma_K$. Indeed, from (13), it is easy to check $\bar{\mathcal{Q}}_E(\boldsymbol{\gamma})$ is invariant under any permutation of the elements of $\boldsymbol{\gamma}$, since $\mathbf{U}\mathbf{\Gamma}\mathbf{U}^\dagger$ has the same distribution as $\mathbf{U}\mathbf{P}\mathbf{\Gamma}\mathbf{P}^\dagger\mathbf{U}^\dagger$ for any permutation matrix $\mathbf{P}$. We recall $\{\sigma_i\}_{1\leq i\leq K}$ are the average channel gains between Alice and Eve as defined in (4).

Proposition 1. *When* $M \geq K \geq n$, $\gamma_1 \geq \cdots \geq \gamma_n > 0$ *and* $\gamma_{n+1} = \cdots = \gamma_K = 0$, $\bar{\mathcal{Q}}_E(\boldsymbol{\gamma})$ *is given as*

$$\bar{\mathcal{Q}}_E(\boldsymbol{\gamma}) = \sum_{j=K-n}^{K-1}\log\frac{\Gamma(K+1-j)\Gamma(j+1)\Gamma(M-K+1)}{\Gamma(K+1)\Gamma(M-K+j+1)} + \log\left(\frac{\det[\mathcal{A}]}{\Delta_K(\boldsymbol{\sigma})\Delta_n(\boldsymbol{\gamma})\prod_{i=1}^n\gamma_i^{K-n}}\right), \tag{15}$$

where the $K \times K$ *matrix* $\mathcal{A}$ *is given by*

$$\mathcal{A} = \left[\{\sigma_i^{j-1}\}_{\substack{1\leq i\leq K\\1\leq j\leq K-n}}, \left\{_2F_0\left(\begin{array}{c}M-K+1,-K\\-\end{array}\middle| -\sigma_i\gamma_j\right)\right\}_{\substack{1\leq i\leq K\\1\leq j\leq n}}\right]. \tag{16}$$

Proof: The proof of Proposition 1 is in Appendix A.

Proposition 2. *When $K > M \geq n$, $\gamma_1 \geq \cdots \geq \gamma_n > 0$ and $\gamma_{n+1} = \cdots = \gamma_K = 0$, $\bar{\mathcal{Q}}_E(\boldsymbol{\gamma})$ is given as*

$$\bar{\mathcal{Q}}_E(\boldsymbol{\gamma}) = \sum_{j=K-n}^{K-1} \log \frac{\Gamma(K+1-j)\Gamma(j+1)}{\Gamma(M+1)\Gamma(M-K+j+1)\Gamma(K-M+1)} + \log \frac{\det[\mathcal{B}]}{\Delta_n(\boldsymbol{\gamma})\Delta_K(\boldsymbol{\sigma})\prod_{i=1}^{n}\gamma_i^{M-n}}, \quad (17)$$

where the $K \times K$ matrix $\mathcal{B}$ is given by

$$\mathcal{B} = \left[\left\{\sigma_i^{j-1}\right\}_{\substack{1 \leq i \leq K \\ 1 \leq j \leq K-n}}, \left\{\sigma_i^{K-M} \,_3F_1\left(\begin{matrix} 1,1,-M \\ K-M+1 \end{matrix}\middle| -\sigma_i\gamma_j\right)\right\}_{\substack{1 \leq i \leq K \\ 1 \leq j \leq n}} \right]. \quad (18)$$

When $K > n > M$, $\bar{\mathcal{Q}}_E(\boldsymbol{\gamma})$ is given as

$$\bar{\mathcal{Q}}_E(\boldsymbol{\gamma}) = \sum_{j=n-M}^{n-1} \log \frac{\Gamma(n+1-j)\Gamma(K-n+j+1)}{\Gamma(M+1)\Gamma(K-M+1)\Gamma(M-n+j+1)} + \log \frac{(-1)^{(K-M)(n-M)}\det[\mathcal{C}]}{\Delta_n(\boldsymbol{\gamma})\Delta_K(\boldsymbol{\sigma})}, \quad (19)$$

where the $(K+n-M) \times (K+n-M)$ matrix $\mathcal{C}$ is given by

$$\mathcal{C} = \begin{bmatrix} \{0\}_{\substack{1 \leq i \leq K-M \\ 1 \leq j \leq n-M}} & \left\{\sigma_j^{i-1}\right\}_{\substack{1 \leq i \leq K-M \\ 1 \leq j \leq K}} \\ \left\{\gamma_i^{j-1}\right\}_{\substack{1 \leq i \leq n \\ 1 \leq j \leq n-M}} & \left\{\gamma_i^{n-M}\sigma_j^{K-M} \,_3F_1\left(\begin{matrix} 1,1,-M \\ K-M+1 \end{matrix}\middle| -\sigma_j\gamma_i\right)\right\}_{\substack{1 \leq i \leq n \\ 1 \leq j \leq K}} \end{bmatrix}. \quad (20)$$

Proof: The proof of Proposition 2 is provided in Appendix B.

According to the definition (14), the generalized hypergeometric functions in (16), (18), and (20) reduce to finite series summations given as

$$_2F_0\left(\begin{matrix} M-K+1, -K \\ - \end{matrix}\middle| -x\right) = \sum_{l=0}^{K} \frac{\Gamma(M-K+l+1)\Gamma(K+1)\, x^l}{\Gamma(M-K+1)\Gamma(K+1-l)\Gamma(l+1)},$$

$$_3F_1\left(\begin{matrix} 1,1,-M \\ K-M+1 \end{matrix}\middle| -x\right) = \sum_{l=0}^{M} \frac{\Gamma(l+1)\Gamma(M+1)\Gamma(K-M+1)\, x^l}{\Gamma(K-M+1+l)\Gamma(M+1-l)}.$$

The Propositions 1 and 2 can be used to compute $\bar{\mathcal{Q}}_E$ when the power allocation $\boldsymbol{\Gamma}$ is rank deficient, i.e., $n < K$. The rank deficiency of $\boldsymbol{\Gamma}$ may be due to the power optimization process when Alice does not allocate power to certain eigen-channels, so as to reduce the information leak towards Eve. As an example, when the number of nodes in Bob is less than the nodes in Alice, i.e., when $N < K$, the main channel $\mathbf{H}$ has null space with dimension $K - N$. The rank of the optimal $\boldsymbol{\Gamma}$ is at most N, since otherwise transmitting information over the null space of $\mathbf{H}$ does not contribute to the secrecy rate.
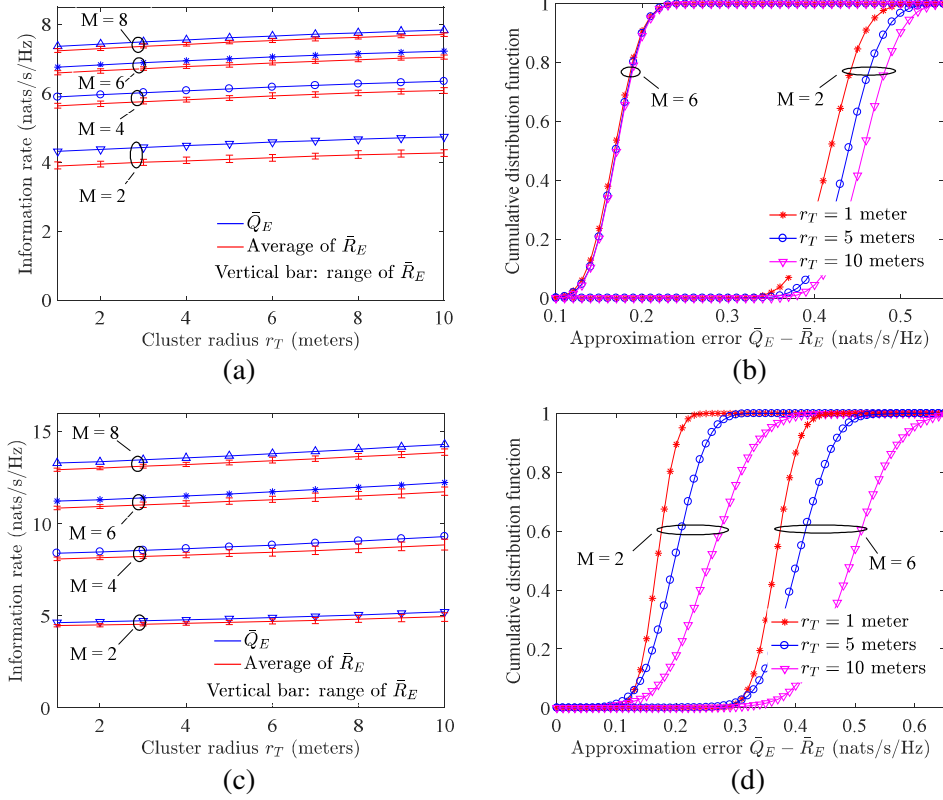
Fig. 2. Comparisons between $\overline{R}_E$ and $\bar{\mathcal{Q}}_E$. The distance between the head of Alice and Eve is $d_E = 30$ meters and the cluster radius of Alice is from $r_T = 1$ to 10 meters. The locations of the transmit nodes and the power loading vector $\boldsymbol{\gamma}$ are random generated. Vertical bars in (a) and (c) denote the range of $\overline{R}_E$ due to different precoding matrix $\mathbf{V}_1$. (a) $\bar{\mathcal{Q}}_E$ and range of $\overline{R}_E$ with $K = 2$; (b) CDFs of approximation error $\bar{\mathcal{Q}}_E - \overline{R}_E$ with $K = 2$; (c) $\bar{\mathcal{Q}}_E$ and range of $\overline{R}_E$ with $K = 6$; (d) CDFs of approximation error $\bar{\mathcal{Q}}_E - \overline{R}_E$ with $K = 6$.

B. Examples of Numerical Results

In this subsection, we present numerical results to validate the approximation $\bar{\mathcal{Q}}_E$ for the average rate $\overline{R}_E$, where $\bar{\mathcal{Q}}_E$ is calculated by (15) when $K \leq M$, and by (17) and (19) when $K > M$. In specific, we illustrate the variation range of $\overline{R}_E$ in Fig. 2 (a) and (c) as the vertical bars, i.e., the length of each bar is $\max \overline{R}_E - \min \overline{R}_E$ under the corresponding system setting. The variation of $\overline{R}_E$ is evaluated by taking 10^4 samples of the precoding matrices $\mathbf{V}_1$, a.k.a., 10^4 samples of the main channel $\mathbf{H}$. Recall that the information rate $\overline{R}_E$ is calculated in (12) by

averaging the eavesdropping channel coefficients $\mathbf{W}$ only, while the precoding $\mathbf{V}_1$ is fixed. The values of $\bar{R}_E$ is then compared with the corresponding $\bar{\mathcal{Q}}_E$. In Fig. 2 (b) and (d), we plot the Cumulative Distribution Function (CDF) of the approximation error $\bar{\mathcal{Q}}_E - \bar{R}_E$, which is induced by replacing the fixed $\mathbf{V}_1$ in $\bar{R}_E$ with the random Haar unitary matrix $\mathbf{U}$ in $\bar{\mathcal{Q}}_E$. When forming the cooperative MIMO system, the transmit nodes are randomly distributed in a circular area with the radius r_T from 1 to 10 meters. The distance between the transmit head node and Eve is set to $d_E = 30$ meters. The number of receive antennas at Eve is assumed to be $M = 2$, 4, 6, or 8, while the number of transmitters at Alice is set to $K = 2$ or 6, where in each case the power allocation vector $\boldsymbol{\gamma}$ is randomly chosen and fixed for the evaluations.

When $r_T = 1$, the transmit nodes are distributed within a small area and their path losses towards Eve have similar value. In this case, the diagonal matrix $\boldsymbol{\Sigma}$ can be approximated as a scaled identity matrix and therefore, $\bar{\mathcal{Q}}_E$ behaves as the strict upper bound of $\bar{R}_E$. The corresponding CDF curves in Fig. 2 (b) and (d) show that the approximation error $\bar{\mathcal{Q}}_E - \bar{R}_E$ can be bounded within 0.5 nats/s/Hz. As the cluster radius increases, the transmit nodes are distributed in a larger area and the values of the elements of $\boldsymbol{\Sigma}$ are more dispersive. When r_T increases to 10 meters, the approximation error can be up-to 0.6 nats/s/Hz when there are 2 transmit nodes, and up-to 0.7 nats/s/Hz when there are 6 transmit nodes. Overall, the approximation $\bar{\mathcal{Q}}_E$ of the average rate $\bar{R}_E$ is reasonably accurate, especially when K and M are large. In all the considered cases, the approximation $\bar{\mathcal{Q}}_E$ over-estimates the corresponding $\bar{R}_E$ with a large probability, i.e., the probability with negative approximation error is not visible in Fig. 2. Therefore, in the context of the physical layer security, it is relevant to use $\bar{\mathcal{Q}}_E$ as an approximation of $\bar{R}_E$ in (11) as it yields the lower bound of the achievable secrecy rate. Using such a lower bound to configure the information rate of the cooperative MIMO transmissions would not violate the secrecy constraint.

IV. TRANSMIT POWER OPTIMIZATION

The secrecy rate maximization (10) is a non-convex problem and its global optimal solution is hard to obtain in general. In this section, we propose to solve an approximate power allocation

problem by replacing $\overline{R}_E(\boldsymbol{\gamma})$ in (11) with its approximation $\bar{\mathcal{Q}}_E(\boldsymbol{\gamma})$ in (13). We further approximate $\bar{\mathcal{Q}}_E(\boldsymbol{\gamma})$ with its affine Taylor expansion based on the closed-form expressions given in Propositions 1 and 2. The Taylor expansions are iteratively updated to find the optimal solution of the original problem (10). Since the affine Taylor expansions are linear, the approximate power allocation problem becomes convex in each iteration, which can be efficiently obtained using standard convex optimization tools.

A. Iterative Power Optimization

First, we present the procedures to obtain the affine Taylor expansions of $\bar{\mathcal{Q}}_E(\boldsymbol{\gamma})$ based on its expressions given by (15), (17), and (19). Given a particular power allocation vector $\boldsymbol{\gamma}_0 \in \mathcal{P}$, the affine Taylor expansion of $\bar{\mathcal{Q}}_E(\boldsymbol{\gamma})$ in a neighborhood of $\boldsymbol{\gamma}_0$ is given by

$$\bar{\mathcal{Q}}_E(\boldsymbol{\gamma}) \approx \bar{\mathcal{Q}}_E(\boldsymbol{\gamma}_0) + \mathbf{g}^{\mathrm{T}}(\boldsymbol{\gamma}_0)(\boldsymbol{\gamma} - \boldsymbol{\gamma}_0), \tag{21}$$

where $\mathbf{g}(\boldsymbol{\gamma}_0) = \left[\frac{\partial}{\partial \gamma_1} \bar{\mathcal{Q}}_E(\boldsymbol{\gamma}), \dots, \frac{\partial}{\partial \gamma_K} \bar{\mathcal{Q}}_E(\boldsymbol{\gamma})\right]^{\mathrm{T}}_{\boldsymbol{\gamma}=\boldsymbol{\gamma}_0}$ denotes the gradient of $\bar{\mathcal{Q}}_E(\boldsymbol{\gamma})$ at $\boldsymbol{\gamma}_0$. When $M \geq K$, $\bar{\mathcal{Q}}_E(\boldsymbol{\gamma})$ is given by (15) and the derivative $\frac{\partial}{\partial \gamma_i} \bar{\mathcal{Q}}_E(\boldsymbol{\gamma})$ can be obtained by using the Jacobi's formula [39] as

$$\frac{\partial}{\partial \gamma_i} \bar{\mathcal{Q}}_E(\boldsymbol{\gamma}) = \frac{\partial}{\partial \gamma_i} \left\{\log \det[\mathcal{A}] - \log \det[\mathbf{V}(\boldsymbol{\gamma})] - (K-n)\log(\gamma_i)\right\}$$

$$= \operatorname{tr}\left(\mathcal{A}^{-1} \frac{\partial}{\partial \gamma_i} \mathcal{A}\right) - \operatorname{tr}\left(\mathbf{V}(\boldsymbol{\gamma})^{-1} \frac{\partial}{\partial \gamma_i} \mathbf{V}(\boldsymbol{\gamma})\right) - \frac{K-n}{\gamma_i}, \tag{22}$$

where $\mathbf{V}(\boldsymbol{\gamma}) = \left\{\gamma_i^{j-1}\right\}_{1 \leq i \leq n, 1 \leq j \leq n}$ denotes the Vandermonde matrix, and the partial derivative of a $a \times a$ matrix $\mathbf{A}(t)$ with respect to the variable t is defined as

$$\tfrac{\partial}{\partial t} \mathbf{A}(t) = \left[\left\{\tfrac{\partial}{\partial t} \mathbf{A}_{i,j}(t)\right\}_{1 \leq i \leq a, 1 \leq j \leq a}\right].$$

Inserting (16) into (22) and applying Laplace expansion of the determinants, we obtain

$$\frac{\partial}{\partial \gamma_i} \bar{\mathcal{Q}}_E(\boldsymbol{\gamma}) = \frac{K(M-K+1)}{\det[\mathcal{A}]} \sum_{j=1}^{K} \frac{\sigma_j M_{j,K-n+i}^{\mathcal{A}}}{(-1)^{K-n+i+j}} \; {}_2F_0\left(\left.\begin{matrix} M-K+2, 1-K \\ - \end{matrix}\right| -\sigma_j \gamma_i\right)$$

$$- \frac{1}{\det[\mathbf{V}(\boldsymbol{\gamma})]} \sum_{j=1}^{n} (-1)^{i+j} M_{j,i}^{\mathbf{V}} \gamma_i^{j-2} - \frac{K-n}{\gamma_i}, \tag{23}$$

where $M_{a,b}^{\mathcal{A}}$ and $M_{a,b}^{\mathbf{V}}$ are the (a,b) minors of the matrices $\mathcal{A}$ and $\mathbf{V}(\boldsymbol{\gamma})$, respectively. In (23), we applied the derivative formula [40, Eq. (16.3.1)].

Similarly, when $K > M \geq n$, the derivative $\frac{\partial}{\partial \gamma_i} \bar{\mathcal{Q}}_E(\boldsymbol{\gamma})$ can be obtained by using (17) as

$$
\frac{\partial}{\partial \gamma_i} \bar{\mathcal{Q}}_E(\boldsymbol{\gamma}) = \operatorname{tr}\left(\mathcal{B}^{-1} \frac{\partial}{\partial \gamma_i} \mathcal{B}\right) - \operatorname{tr}\left(\mathbf{V}(\boldsymbol{\gamma})^{-1} \frac{\partial}{\partial \gamma_i} \mathbf{V}(\boldsymbol{\gamma})\right) - \frac{M-n}{\gamma_i}
$$

$$
= \frac{M}{(K-M+1)\det[\mathcal{B}]} \sum_{j=1}^{K} \frac{\sigma_j^{K-M+1} M_{j,K-n+i}^{\mathcal{B}}}{(-1)^{K-n+i+j}} \; {}_3F_1\left(\begin{matrix}2,2,1-M\\K-M+2\end{matrix}\middle| -\sigma_j\gamma_i\right)
$$

$$
- \frac{1}{\det[\mathbf{V}(\boldsymbol{\gamma})]} \sum_{j=1}^{n} (-1)^{i+j} M_{j,i}^{\mathbf{V}} \gamma_i^{j-2} - \frac{M-n}{\gamma_i}.
$$

When $K > n > M$, the derivative $\frac{\partial}{\partial \gamma_i} \bar{\mathcal{Q}}_E(\boldsymbol{\gamma})$ is obtained by using (19) as

$$
\frac{\partial}{\partial \gamma_i} \bar{\mathcal{Q}}_E(\boldsymbol{\gamma}) = \operatorname{tr}\left(\mathcal{C}^{-1} \frac{\partial}{\partial \gamma_i} \mathcal{C}\right) - \operatorname{tr}\left(\mathbf{V}(\boldsymbol{\gamma})^{-1} \frac{\partial}{\partial \gamma_i} \mathbf{V}(\boldsymbol{\gamma})\right)
$$

$$
= \frac{1}{\det[\mathcal{C}]} \sum_{j=1}^{n-M} \frac{(j-1) M_{j,K-M+i}^{\mathcal{C}}}{(-1)^{K-M+i+j}} \gamma_i^{j-2} - \frac{1}{\det[\mathbf{V}(\boldsymbol{\gamma})]} \sum_{j=1}^{n} (-1)^{i+j} M_{j,i}^{\mathbf{V}} \gamma_i^{j-2}
$$

$$
+ \frac{n-M}{\det[\mathcal{C}]} \sum_{j=1}^{K} \frac{\gamma_i^{n-M-1} \sigma_j^{K-M} M_{n-M+j,K-M+i}^{\mathcal{C}}}{(-1)^{K-2M+n+i+j}} \; {}_3F_1\left(\begin{matrix}1,1,-M\\K-M+1\end{matrix}\middle| -\sigma_j\gamma_i\right)
$$

$$
+ \frac{M}{(K-M+1)\det[\mathcal{C}]} \sum_{j=1}^{K} \frac{\gamma_i^{n-M} \sigma_j^{K-M+1} M_{n-M+j,K-M+i}^{\mathcal{C}}}{(-1)^{K-2M+n+i+j}} \; {}_3F_1\left(\begin{matrix}2,2,1-M\\K-M+2\end{matrix}\middle| -\sigma_j\gamma_i\right).
$$

Next, the affine Taylor expansion of $\bar{\mathcal{Q}}_E(\boldsymbol{\gamma})$ is substituted into (11) and the optimization function $R_s(\boldsymbol{\gamma})$ can be approximated in a neighborhood of $\boldsymbol{\gamma}_0 \in \mathcal{P}$ as

$$
R_s(\boldsymbol{\gamma}) \approx \widetilde{R_s}(\boldsymbol{\gamma}, \boldsymbol{\gamma}_0) = \sum_{i=1}^{K} \log\left(1 + \frac{\gamma_B}{\gamma_E} \bar{\lambda}_i \gamma_i\right) - \max_{1 \leq i \leq L}\left[\bar{\mathcal{Q}}_{E,i}(\boldsymbol{\gamma}_0) + \mathbf{g}_i^{\mathrm{T}}(\boldsymbol{\gamma}_0)(\boldsymbol{\gamma} - \boldsymbol{\gamma}_0)\right]. \quad (24)
$$

As the first term of (24) is a concave function of $\boldsymbol{\gamma}$ and the second term is linear, $\widetilde{R_s}(\boldsymbol{\gamma}, \boldsymbol{\gamma}_0)$ is a concave function of $\boldsymbol{\gamma}$. Together with the linear constraint $\sum_{i=1}^{K} \gamma_i \leq \gamma_E$, the maximization of the function $\widetilde{R_s}(\boldsymbol{\gamma}, \boldsymbol{\gamma}_0)$, in a neighborhood around $\boldsymbol{\gamma}_0$, can be efficiently solved by standard convex programming tools, such as CVX [41], [42].

Finally, following similar procedures as described in [43], the non-convex secrecy rate maximization problem (10) is converted into a sequence of concave maximization sub-problems. Specifically, selecting an initial point $\boldsymbol{\gamma}_0 \in \mathcal{P}$, the kth sub-problem, $k \geq 1$, is given as

$$
\boldsymbol{\gamma}_k = \arg\max_{\boldsymbol{\gamma} \in \mathcal{P}} \left[\widetilde{R_s}(\boldsymbol{\gamma}, \boldsymbol{\gamma}_{k-1})\right]^+, \quad \text{s.t. } \sum_{i=1}^{K} \gamma_i \leq \gamma_E, \quad (25)
$$

where $\boldsymbol{\gamma}_k$ denotes the optimal solution of the kth sub-problem. Consider the consecutive $(k+1)^{st}$ and k^{th} sub-problems, where $\boldsymbol{\gamma}_{k-1}$, $\boldsymbol{\gamma}_k$, and $\boldsymbol{\gamma}_{k+1}$ are all feasible solutions. We have the following chain of inequalities $\widetilde{R_s}(\boldsymbol{\gamma}_{k+1}, \boldsymbol{\gamma}_k) \geq \widetilde{R_s}(\boldsymbol{\gamma}_k, \boldsymbol{\gamma}_k) \geq \widetilde{R_s}(\boldsymbol{\gamma}_k, \boldsymbol{\gamma}_{k-1})$, i.e., the secrecy

rate $\widetilde{R}_s$ is monotonically increasing. We will demonstrate in the next subsection how the secrecy rate improves as the number of iterative steps increases.

The initial power allocation vector $\boldsymbol{\gamma}_0$ is selected as the solution of the water-filling algorithm, which only maximizes the information rate between Alice and Bob, i.e., $\boldsymbol{\gamma}_{\mathrm{WF}} = \arg\max\left\{\sum_{i=1}^{K}\log\left(1 + \frac{\gamma_B}{\gamma_E}\bar{\lambda}_i\gamma_i\right) : \boldsymbol{\gamma} \in \mathcal{P}, \ \sum_{i=1}^{K}\gamma_i \leq \gamma_E\right\}$. The iterative power optimization procedures is summarized in Algorithm 1. As shown in line 4, the algorithm terminates when the secrecy rate improvement between consecutive sub-problems is less than a threshold ϵ.

Algorithm 1: Iterative Power Optimization

1: **Initialize:** $\boldsymbol{\gamma}_0 = \boldsymbol{\gamma}_{\mathrm{WF}}$
2: **for** $k \geq 1$ **do**
3:    Solve the convex sub-problem (25) with CVX.
4:    **if** $\widetilde{R}_s(\boldsymbol{\gamma}_k, \boldsymbol{\gamma}_{k-1}) - \widetilde{R}_s(\boldsymbol{\gamma}_{k-1}, \boldsymbol{\gamma}_{k-2}) \geq \varepsilon$ **then**
5:        $k \to k+1$, **continue**
6:    **else**
7:        Set the output $\boldsymbol{\gamma}^* = \boldsymbol{\gamma}_k$, **return**
8:    **end if**
9: **end for**

B. Numerical Results

To illustrate the convergence of the Algorithm 1, we present the sequence of the optimized rates $\left\{\widetilde{R}_s(\boldsymbol{\gamma}_k, \boldsymbol{\gamma}_{k-1})\right\}_{k\geq 1}$ achieved in each step of the iterative power optimizations. We consider two cooperative MIMO channels in presence of an eavesdropper with multiple possible locations. In the first case, we assume $K = N = 2$ legitimate transmit and receive nodes, where the channel coefficients of the main channel $\mathbf{H}_1$ are given as follows

$$\mathbf{H}_1 = \begin{bmatrix} 1.97 - 0.92i & 0.98 + 0.47i \\ -0.63 - 0.035i & 0.019 - 1.24i \end{bmatrix}. \tag{26}$$

In the second case, we assume $K = N = 4$ with the channel coefficients given as

$$\mathbf{H}_2 = \begin{bmatrix} 1.09 - 0.28i & 0.27 - 0.85i & 1.65 - 1.43i & 1.01 - 0.68i \\ -0.51 + 0.77i & 0.092 + 0.26i & 0.45 - 1.003i & -0.303 + 0.057i \\ 0.28 - 1.09i & -0.58 - 0.44i & 0.25 + 1.31i & -0.42 - 0.66i \\ 0.64 + 0.94i & 0.74 + 0.62i & 0.18 - 0.75i & 0.401 + 0.11i \end{bmatrix}. \tag{27}$$
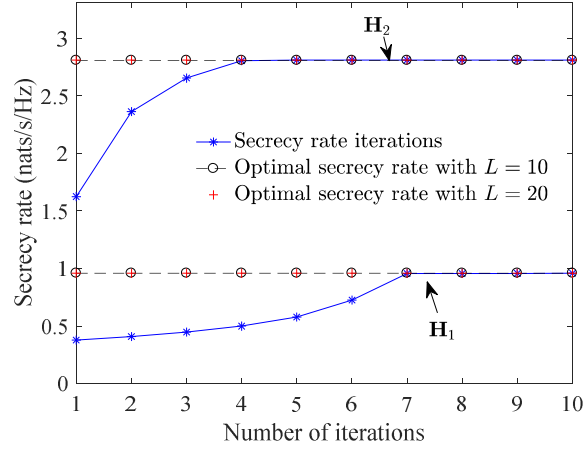
Fig. 3. Convergence of the secrecy rate for the iterative power optimization Algorithm 1. The sample channels between the legitimate nodes are chosen as $\mathbf{H}_1$ in (26) and $\mathbf{H}_2$ in (27).

In both cases, the eavesdropper is equipped with 2 receive antennas and can appear at $L = 10$ or 20 possible locations, which are uniformly placed on a circle with equal distance $d_E = 30$ meters towards the transmit head node. In Fig. 3, the secrecy rates obtained in each iteration of the power optimization are plotted for the cooperative MIMO channels $\mathbf{H}_1$ and $\mathbf{H}_2$. As a comparison, the optimal achievable secrecy rates are also obtained by numerically searching over the space of the power allocation vectors. Over the channels $\mathbf{H}_1$ and $\mathbf{H}_2$, the secrecy rate converges fast to the corresponding optimal values with 7 and 4 iterations, respectively. In both cases, the secrecy rates monotonically increase, which is in line with our prediction in Section IV-A. In addition, we also observe that a larger number of Eve's locations does not change the resulting optimal secrecy rate. Therefore, we will fix $L = 10$ in the following numerical evaluations.

Next, we investigate the achievable secrecy rate when the cluster heads can flexibly change the number of legitimate assisting nodes, which are located within a given cluster radius. We assume there always exists enough number of assisting nodes as requested by the head node. The number of legitimate nodes in each cluster is allowed to vary from 1 to 6, while the number of antennas at Eve is fixed to 4. The distance between the legitimate head nodes is set to $d_B = 30$ meters and the distance between Eve and the transmit head node can be $d_E = 25, 30,$ or 35 meters. The achievable secrecy rate is evaluated when the legitimate nodes are distributed in clusters with radius 5 or 8 meters. As shown in Fig. 4, when only one legitimate node (the head node itself) is
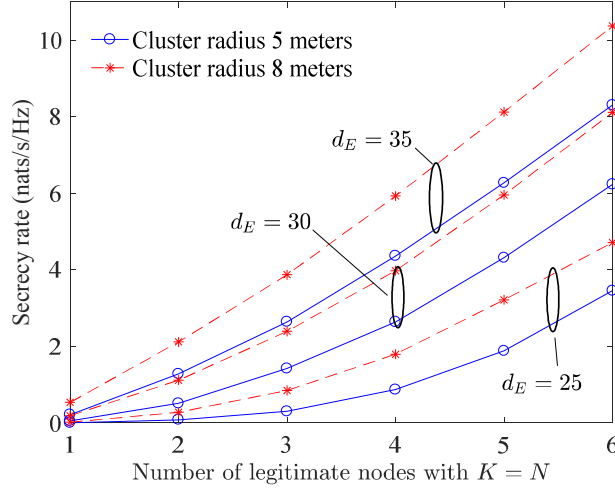
Fig. 4. Secrecy rate R_{sec} with equal number of legitimate nodes in transmit and receive clusters, where $M = 4$, $d_B = 30$ meters and $d_E = 25, 30,$ or 35 meters. Solid lines: secrecy rate with cluster radius 5 meters; dashed lines: secrecy rate with cluster radius 8 meters.

used in each cluster, only a marginal secrecy rate can be achieved in the considered settings. By increasing the number of cooperative nodes, the secrecy rate can be efficiently improved, even when Eve is closer to Alice. In the cases with $d_E = 25$, the rate improvement is less significant when K and N are less than M, while the rate improvement increases when K and N exceed M. When d_E become 30 and 35 meters, the secrecy rates tend to be linearly increased. Fig. 4 also shows that the secrecy rate can be further improved by increasing the cluster radius.

In the following numerical results, we study the impacts of the cluster radius on the secrecy rate of the cooperative MIMO systems in more detail. The secrecy rate is evaluated when K legitimate transmit nodes and N legitimate receive nodes are distributed in the corresponding cluster areas with the cluster radius ranging from 1 to 10 meters, where we set $K = 4$ and $N = 4$ or 6. The distance between the head nodes of Alice and Bob is set to $d_B = 30$ meters. In Fig. 5 (a), the number of antennas at Eve is $M = 2$, less than K and N, while Eve is allowed to be closer to Alice with $d_E = 20$ or 30 meters. In these settings, it is observed that a significant secrecy rate can be achieved even when $d_E < d_B$. This advantageous secrecy rate is achieved due to the degree-of-freedom advantage of the legitimate nodes as opposed to the eavesdropper. As the cluster radius increases, the legitimate nodes are distributed more dispersively within their
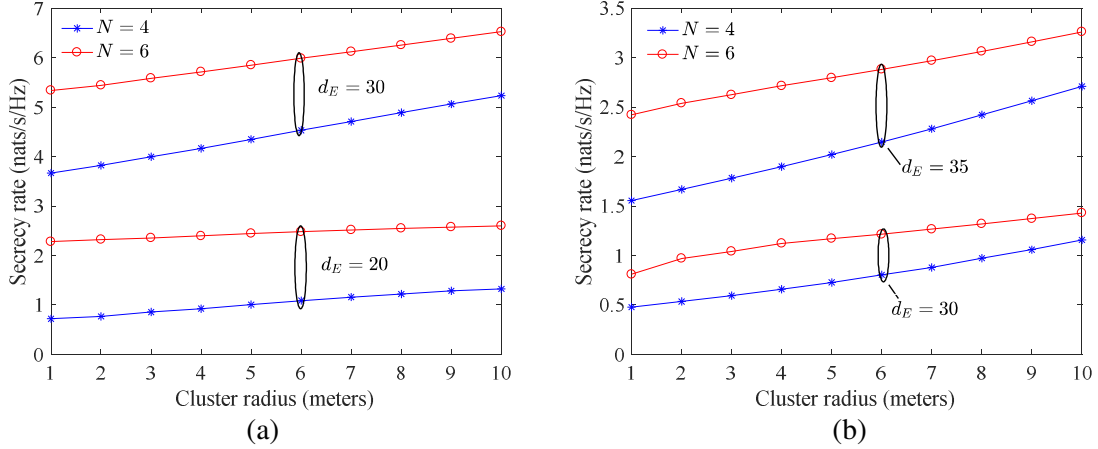
Fig. 5. Secrecy rate R_{sec} with $K = 4$ and $N = 4$ or 6, with distance between head nodes of Alice and Bob being $d_B = 30$ meters. The number of antennas at Eve is $M = 2$ in (a) and $M = 6$ in (b). In (a), the distance between Alice and Eve $d_E = 20$ or 30 meters, while in (b) $d_E = 30$ or 35 meters.

corresponding clusters, and thus, could reduce the distance between some of the legitimate transmitters and receivers. Therefore, the secrecy rate improves as the cluster radius increases, which is especially visible when $d_E = 30$ meters. It is noted that although Bob with $N = 6$ receive nodes achieves higher secrecy rate, as the radius increases, the rate improvement is less significant compared to the case $N = 4$. It is due to the fact that the additional receive nodes are located further from Alice (e.g., the rightmost node of Bob in Fig. 1). Increasing the cluster radius also increases the distance between these nodes and the nodes in Alice, which results in smaller secrecy rate improvement. In Fig. 5 (b), we compare the achievable secrecy rate when Eve has equal or more antennas compared to the number of legitimate nodes at Alice and Bob. Specifically, we assume $M = 6$ antenna elements at Eve, while the distance between Alice and Eve is $d_E = 30$ or 35 meters. In these settings, when the distances d_B and d_E are equal and $N = 4$, i.e., the legitimate receiver has inferior capability in terms of the number of antennas, only marginal secrecy rate can be obtained when the cluster radius is small. By increasing the cluster radius, the secrecy rate is improved, almost linearly proportional to the cluster radius. In addition, the secrecy rate can be improved more effectively when $d_E = 35$ meters, i.e., when the legitimate receiver has distance advantage. As a comparison, by increasing both the cluster radius and the number of nodes at Bob, the secrecy rates can be improved by 1 nats/s/Hz when $d_E = 30$ and by 1.7

nats/s/Hz when $d_E = 35$.

V. CONCLUSIONS

As the small footprint mobile devices can be only equipped with limited number of antenna, the secrecy communications between such devices is difficult to realize when the eavesdropper has more antennas and experiences superior SNR. The proposed secrecy cooperative MIMO architecture resolves this issue by temporally activating nearby trusted mobile devices to form cooperative cluster and jointly transmit or receive confidential message, where the communications between clusters resemble a distributed MIMO system. The secrecy cooperative MIMO architecture aims to enable and improve the secrecy transmissions, by activating a sufficiently large number of trusted devices and shortening the average distance between the legitimate transceivers.

The eigen-direction precoding is applied to construct the input signal and the secrecy rate is obtained, when the eavesdropper may be located at arbitrary number of possible representative locations. By using Random Matrix Theory, we obtain accurate approximation for the average rate between Alice and Eve. The proposed approximations enable the linear affine representations of the information rate between Alice and Eve. By using the affine representations, the non-convex secrecy rate optimization, against multiple possible locations of Eve, is recast into a sequence of convex sub-problems, which can be efficiently solved by standard convex optimization tools. Results show that the achievable secrecy rate can be improved quite effectively by enabling more trusted devices in each cooperative cluster compared to the number of antennas at Eve, i.e., when Alice and Bob outperform Eve in terms of the available spatial degrees of freedom. By increasing the radius of cooperative clusters, the secrecy rate can be further improved due to shorter average distance between legitimate nodes.

APPENDIX A

PROOF OF PROPOSITION 1

The proofs of Propositions 1 and 2 relies on the following lemmas.

Lemma 1 (*l'Hôpital's rule* [36]). *Consider the ratio of determinants of the form* $\det[f_i(z_j)]/\Delta_a(z)$, *where the row index* i *and the column index* j *run from 1 to* a *and the vector* $z = [z_1, ..., z_a]$. *As* $z_{b+1}, ..., z_a$ *($b \leq a$) approach zero, the limit of the ratio is given by*

$$\lim_{z_{b+1},\dots,z_a \to 0} \frac{\det[f_i(z_j)]}{\Delta_a(\boldsymbol{z})} = \frac{\det\left[\left\{f_i^{(j-1)}(z)\big|_{z=0}\right\}_{\substack{1\le i\le a\\1\le j\le a-b}} \quad \{f_i(z_j)\}_{\substack{1\le i\le a\\1\le j\le b}}\right]}{\Delta_b(\boldsymbol{z})\prod_{i=1}^{b}z_i^{a-b}\prod_{j=1}^{a-b-1}j!}, \tag{28}$$

where $f^{(m)}(z)$ denotes the mth derivative of $f(z)$.

Lemma 2 (*Generalized Andréief integral* [44]). *Consider the integral*

$$\mathcal{J} = \int_{\mathbb{C}^L} \det\left[\begin{array}{c}\{r_{i,j}\}_{\substack{1\le i\le a\\1\le j\le L+a}}\\ \{R_j(z_i)\}_{\substack{1\le i\le L\\1\le j\le L+a}}\end{array}\right] \det\left[\begin{array}{c}\{s_{i,j}\}_{\substack{1\le i\le b\\1\le j\le L+b}}\\ \{S_j(z_i)\}_{\substack{1\le i\le L\\1\le j\le L+b}}\end{array}\right] dz_1 \dots dz_L,$$

where the functions $R_j(\cdot)$ *and* $S_j(\cdot)$ *are such that the integral is convergent. Then, the following identity holds:*

$$\mathcal{J} = (-1)^{ab}L!\det\left[\begin{array}{cc}\{0\}_{\substack{1\le i\le b\\1\le j\le a}} & \{s_{i,j}\}_{\substack{1\le i\le b\\1\le j\le L+b}}\\ \{r_{j,i}\}_{\substack{1\le i\le L+a\\1\le j\le a}} & \left\{\int_{\mathbb{C}} R_i(z)S_j(z)\,dz\right\}_{\substack{1\le i\le L+a\\1\le j\le L+b}}\end{array}\right]. \tag{29}$$

We are now ready to prove Proposition 1. Consider the quantity

$$\phi(s) = \mathbb{E}[\det(\mathbf{I}+\mathbf{F}\mathbf{U}\boldsymbol{\Gamma}\mathbf{U}^\dagger\mathbf{F}^\dagger)^s],$$

where s is an arbitrary real number. By definition, $\phi(s)$ is known as the moment generating function of the random variable $\log\det(\mathbf{I}+\mathbf{F}\mathbf{U}\boldsymbol{\Gamma}\mathbf{U}^\dagger\mathbf{F}^\dagger)$ and the desired quantity $\bar{\mathcal{Q}}_E$ can be obtained as $\bar{\mathcal{Q}}_E = \log\phi(1)$. Using the matrix determinant lemma and the definition $\mathbf{F} = \mathbf{W}\boldsymbol{\Sigma}^{1/2}$, $\phi(s)$ can be rewritten as

$$\phi(s) = \mathbb{E}[\det(\mathbf{I}+\boldsymbol{\Sigma}^{1/2}\mathbf{W}^\dagger\mathbf{W}\boldsymbol{\Sigma}^{1/2}\mathbf{U}\boldsymbol{\Gamma}\mathbf{U}^\dagger)^s]. \tag{30}$$

The matrix $\mathbf{W}$ is complex Gaussian distributed with the density

$$f(\mathbf{W}) = \pi^{-MK}\exp(-\mathrm{tr}\mathbf{W}\mathbf{W}^\dagger). \tag{31}$$

Inserting (31) into (30) and applying the change-of-variables $\mathbf{X} = \mathbf{W}\boldsymbol{\Sigma}^{1/2}$, we obtain

$$\phi(s) = \frac{\int_{\mathcal{U}(K)}\int_{\mathcal{M}(M,K)}\det(\mathbf{I}+\mathbf{X}^\dagger\mathbf{X}\mathbf{U}\boldsymbol{\Gamma}\mathbf{U}^\dagger)^s\exp(-\mathrm{tr}\mathbf{X}^\dagger\mathbf{X}\,\boldsymbol{\Sigma}^{-1})d\mathbf{X}d\mathbf{U}}{\det[\boldsymbol{\Sigma}]^M\int_{\mathcal{M}(M,K)}\exp(-\mathrm{tr}\mathbf{X}^\dagger\mathbf{X})d\mathbf{X}}, \tag{32}$$

where $\mathcal{M}(M,K)$ denotes the space of $M\times K$ complex matrices, $d\mathbf{U}$ denotes the normalized Haar measure on the unitary group $\mathcal{U}(K)$, and $d\mathbf{X}$ defines the measure $d\mathbf{X} = \prod_{i=1}^{M}\prod_{j=1}^{K}\mathfrak{R}(\mathbf{X}_{i,j})\,\mathfrak{I}(\mathbf{X}_{i,j})$. The denominator of (32) normalizes the right-hand-side of (32).

Next, we apply the eigenvalue decomposition $\mathbf{X}^\dagger\mathbf{X} = \mathbf{V}\boldsymbol{\Omega}\mathbf{V}^\dagger$ with the Jacobian given by [45] as $d\mathbf{X} = \Delta_K(\boldsymbol{\omega})^2 \prod_{i=1}^K \omega_i^{M-K} d\boldsymbol{\omega} d\mathbf{V}$, where $d\boldsymbol{\omega} = d\omega_1 \dots d\omega_K$ and $d\mathbf{V}$ is the normalized Haar measure. Then, $\phi(s)$ can be rewritten as

$$\phi(s) = \frac{1}{\det[\boldsymbol{\Sigma}]^M} \frac{\int_{[0,\infty)^K} \Delta_K(\boldsymbol{\omega})^2 \prod_{i=1}^K \omega_i^{M-K} \int_{\mathcal{U}(K)} \exp(-\mathrm{tr}\mathbf{V}\boldsymbol{\Omega}\mathbf{V}^\dagger\boldsymbol{\Sigma}^{-1}) \mathcal{I}_1(\boldsymbol{\Omega},\mathbf{V}) d\mathbf{V} d\boldsymbol{\omega}}{\int_{[0,\infty)^K} \Delta_K(\boldsymbol{\omega})^2 \prod_{i=1}^K \omega_i^{M-K} \exp(-\omega_i) d\boldsymbol{\omega}}, \tag{33}$$

where

$$\mathcal{I}_1(\boldsymbol{\Omega},\mathbf{V}) = \int_{\mathcal{U}(K)} \det(\mathbf{I} + \mathbf{V}\boldsymbol{\Omega}\mathbf{V}^\dagger\mathbf{U}\boldsymbol{\Gamma}\mathbf{U}^\dagger)^s \, d\mathbf{U}. \tag{34}$$

We first solve the integral $\mathcal{I}_1(\boldsymbol{\Omega},\mathbf{V})$ by assuming all the diagonal elements of $\boldsymbol{\Gamma}$ being non-zero, i.e., $n = K$. The general result with $0 < n < K$ is obtained by taking the limit $\gamma_{n+1}, \dots, \gamma_K \to 0$. By using the integral identity [41, Eq. (3.21)], $\mathcal{I}_1(\boldsymbol{\Omega},\mathbf{V})$ can be solved as

$$\mathcal{I}_1(\boldsymbol{\Omega},\mathbf{V}) = \frac{\det[(1+\omega_i\gamma_j)^{s+K-1}]}{\Delta_K(\boldsymbol{\omega})\Delta_K(\boldsymbol{\gamma})} \prod_{j=0}^{K-1} \frac{\Gamma(s+K-j)\Gamma(j+1)}{\Gamma(s+K)}, \tag{35}$$

where the row index i and the column index j in the determinant of (35) run from 1 to K. Using Lemma 1, $\mathcal{I}_1(\boldsymbol{\Omega},\mathbf{V})$ is obtained, with $M \geq K \geq n$, by letting $\gamma_{n+1}, \dots, \gamma_K \to 0$ as

$$\mathcal{I}_1(\boldsymbol{\Omega},\mathbf{V}) = \frac{\det\left[\left\{\omega_i^{j-1}\right\}_{\substack{1\leq i\leq K \\ 1\leq j\leq K-n}} \quad \left\{(1+\omega_i\gamma_j)^{s+K-1}\right\}_{\substack{1\leq i\leq K \\ 1\leq j\leq n}}\right]}{\Delta_K(\boldsymbol{\omega})\Delta_n(\boldsymbol{\gamma})\prod_{i=1}^n \gamma_i^{K-n}} \prod_{j=K-n}^{K-1} \frac{\Gamma(s+K-j)\Gamma(j+1)}{\Gamma(s+K)}. \tag{36}$$

Therefore, the integral $\mathcal{I}_1(\boldsymbol{\Omega},\mathbf{V})$ is independent of the matrix $\mathbf{V}$, i.e., $\mathcal{I}_1(\boldsymbol{\Omega}) \equiv \mathcal{I}_1(\boldsymbol{\Omega},\mathbf{V})$, which can be pulled out of the integral over $\mathbf{V} \in \mathcal{U}(K)$ in (33). The integration over $\mathbf{V}$, denoted as $\mathcal{I}_2(\boldsymbol{\Omega}) = \int_{\mathcal{U}(K)} \exp(-\mathrm{tr}\mathbf{V}\boldsymbol{\Omega}\mathbf{V}^\dagger\boldsymbol{\Sigma}^{-1}) d\mathbf{V}$, can be solved by the Harish-Chandra-Itzykson-Zuber integral formula [47] as follows

$$\mathcal{I}_2(\boldsymbol{\Omega}) = \frac{(\det\boldsymbol{\Sigma})^{K-1}}{\Delta_K(\boldsymbol{\omega})\Delta_K(\boldsymbol{\sigma})} \det\left[\exp\left(-\frac{\omega_i}{\sigma_j}\right)\right] \prod_{j=0}^{K-1} \Gamma(j+1). \tag{37}$$

Moreover, the denominator in (33) is a Selberg integral [43, Eq. (17.6.5)] and solved as

$$\int_{[0,\infty)^K} \Delta(\boldsymbol{\omega})^2 \prod_{i=1}^K \omega_i^{M-K} \exp(-\omega_i) \, d\boldsymbol{\omega} = \prod_{i=1}^K \Gamma(j+1)\Gamma(M-K+j). \tag{38}$$

Note that when $K > M$, (38) is also true by interchanging M and K. Inserting (36)-(38) into (33), we obtain

$$\phi(s) = \frac{1}{K!} \left(\prod_{j=K-n}^{K-1} \frac{\Gamma(s+K-j)\Gamma(j+1)}{\Gamma(s+K)}\right) \left(\prod_{j=1}^K \frac{1}{\Gamma(M-K+j)}\right) \frac{(\det\boldsymbol{\Sigma})^{K-M-1}}{\Delta_n(\boldsymbol{\gamma})\Delta_K(\boldsymbol{\sigma})\prod_{i=1}^n \gamma_i^{K-n}}$$

$$\times \int_{[0,\infty)^K} \prod_{i=1}^K \omega_i^{M-K} \det\left[\left\{\omega_i^{j-1}\right\}_{\substack{1\leq i\leq K \\ 1\leq j\leq K-n}} \quad \left\{(1+\omega_i\gamma_j)^{s+K-1}\right\}_{\substack{1\leq i\leq K \\ 1\leq j\leq n}}\right] \det[e^{-\omega_i/\sigma_j}] \, d\boldsymbol{\omega}$$

$$= \left(\prod_{j=K-n}^{K-1} \frac{\Gamma(s+K-j)\Gamma(j+1)}{\Gamma(s+K)}\right) \left(\prod_{j=1}^{K} \frac{1}{\Gamma(M-K+j)}\right) \frac{(\det \mathbf{\Sigma})^{K-M-1}}{\Delta_n(\boldsymbol{\gamma})\Delta_K(\boldsymbol{\sigma})\prod_{i=1}^{n}\gamma_i^{K-n}}$$

$$\times \det\left[\left\{\sigma_i^{M-K+j}\Gamma(M-K+j)\right\}_{\substack{1\leq i\leq K \\ 1\leq j\leq K-n}} \quad \left\{\int_0^\infty x^{M-K}(1+x\gamma_j)^{s+K-1}\mathrm{e}^{-\frac{x}{\sigma_i}}\,dx\right\}_{\substack{1\leq i\leq K \\ 1\leq j\leq n}}\right], \quad (39)$$

where the second equality is due to Lemma 2. The integrals in the determinant of (39) can be represented as the generalized hypergeometric function as

$$\int_0^\infty x^{M-K}(1+x\gamma_j)^{s+K-1}\mathrm{e}^{-\frac{x}{\sigma_i}}\,dx = \frac{\Gamma(M-K+1)}{\sigma_i^{K-M-1}}\,{}_2F_0\left(\begin{matrix}M-K+1, 1-s-K \\ -\end{matrix}\middle| -\sigma_i\gamma_j\right).$$

By setting $s=1$, and factoring out $\sigma_i^{M-K+1}\Gamma(M-K+j)$ from the 1st to the $(K-n)^{th}$ columns, $\Gamma(M-K+1)\sigma_i^{M-K+1}$ from the last n columns of the determinant on the right-hand-side of (39), we obtain the desired result as in (15).

APPENDIX B

PROOF OF PROPOSITION 2

By following the same procedures as in (30)-(33), we obtain $\phi(s)$ as

$$\phi(s) = \frac{\int_{[0,\infty)^M}\Delta(\boldsymbol{\omega})^2\prod_{i=1}^{M}\omega_i^{K-M}\int_{\mathcal{U}(K)}\exp(-\mathrm{tr}\mathbf{V}\mathbf{\Omega}\mathbf{V}^\dagger\mathbf{\Sigma}^{-1})\mathcal{I}_1(\mathbf{\Omega},\mathbf{V})d\mathbf{V}d\boldsymbol{\omega}}{\det[\mathbf{\Sigma}]^M\int_{[0,\infty)^M}\Delta(\boldsymbol{\omega})^2\prod_{i=1}^{M}\omega_i^{K-M}\exp(-\omega_i)d\boldsymbol{\omega}}, \quad (40)$$

where $\mathcal{I}_1(\mathbf{\Omega},\mathbf{V})$ is given in (34). When $K>M$, the diagonal matrix $\mathbf{\Omega}$, containing the M non-zero eigenvalues of the Hermitian matrix $\mathbf{\Sigma}^{1/2}\mathbf{W}^\dagger\mathbf{W}\mathbf{\Sigma}^{1/2}$, is of the form $\mathbf{\Omega} = \mathrm{diag}([\omega_1,\dots,\omega_M,0,\dots,0])$. Before applying Lemma 1 to (36) to set the corresponding $\omega_{M+1},\dots,\omega_K$ to zero, we have to rewrite $(1+\omega_i\gamma_j)^{s+K-1}$ in (36) to guarantee the convergence of the integral (40). By the generalized binomial expansion, we have

$$(1+\omega_i\gamma_j)^{s+K-1} = \sum_{l=0}^{\infty}\frac{\Gamma(s+K)(\omega_i\gamma_j)^l}{\Gamma(s+K-l)\Gamma(l+1)}, \quad (41)$$

where we assume $|\omega_i\gamma_j|<1$ to guarantee the convergence. We will later on extend this expression to arbitrary values of $\omega_i\gamma_j$. Inserting (41) into (36), we obtain

$$\mathcal{I}_1(\mathbf{\Omega},\mathbf{V}) = \frac{\det\left[\left\{\omega_i^{j-1}\right\}_{\substack{1\leq i\leq K \\ 1\leq j\leq K-n}} \quad \left\{\sum_{l=0}^{\infty}\frac{\omega_i^{K-n}(\omega_i\gamma_j)^l}{\Gamma(s+n-l)\Gamma(K-n+l+1)}\right\}_{\substack{1\leq i\leq K \\ 1\leq j\leq n}}\right]}{\Delta_K(\boldsymbol{\omega})\Delta_n(\boldsymbol{\gamma})\left(\prod_{j=K-n}^{K-1}\Gamma(s+K-j)\Gamma(j+1)\right)^{-1}}, \quad (42)$$

where the first $K-n$ summands in the infinite summations are cancelled as they are the linear combinations of $\left\{\omega_i^{j-1}\right\}_{\substack{1\leq i\leq K \\ 1\leq j\leq K-n}}$. Then, we apply Lemma 1 to (42) to take the limit

$\omega_{M+1}, \dots, \omega_K \to 0$. When $K > M \geq n$, we obtain

$$\mathcal{J}_1(\mathbf{\Omega}, \mathbf{V}) = \frac{\det\left[\{\omega_i^{j-1}\}_{\substack{1 \leq i \leq M \\ 1 \leq j \leq M-n}} \quad \left\{{}_2F_1\binom{1,1-s-M}{K-M+1}\Big|-\omega_i\gamma_j\right\}_{\substack{1 \leq i \leq M \\ 1 \leq j \leq n}}\right]}{\Delta_M(\boldsymbol{\omega})\Delta_n(\boldsymbol{\gamma})\prod_{j=1}^n \gamma_j^{M-n}} \prod_{j=K-n}^{K-1} \frac{\Gamma(s+K-j)\Gamma(j+1)}{\Gamma(s+M)\Gamma(K-M+1)},$$

and when $K > n > M$, we obtain

$$\mathcal{J}_1(\mathbf{\Omega}, \mathbf{V}) = \det\left[\begin{array}{c}\{\gamma_j^{i-1}\}_{\substack{1 \leq i \leq n-M \\ 1 \leq j \leq n}} \\ \left\{\gamma_j^{n-M}\,{}_2F_1\binom{1,1-s-M}{K-M+1}\Big|-\omega_i\gamma_j\right\}_{\substack{1 \leq i \leq M \\ 1 \leq j \leq n}}\end{array}\right] \frac{\prod_{j=n-M}^{n-1}\Gamma(s+n-j)\Gamma(j+K-n+1)}{\Delta_M(\boldsymbol{\omega})\Delta_n(\boldsymbol{\gamma})\Gamma(s+M)^M\Gamma(K-M+1)^M},$$

where we replace the infinite summation with its corresponding hypergeometric representation:

$$\sum_{l=0}^\infty \frac{x^l}{\Gamma(a-l)\Gamma(b+l+1)} = \frac{1}{\Gamma(a)\Gamma(b+1)}\,{}_2F_1\binom{1,1-a}{b+1}\Big|-x\Big).$$

Note that the representation using the hypergeometric function can be analytically continued to arbitrary values of x. Again, we notice that the integral $\mathcal{J}_1(\mathbf{\Omega}, \mathbf{V}) \equiv \mathcal{J}_1(\mathbf{\Omega})$ is independent of the matrix $\mathbf{V}$ and can be pulled out of the integral over $\mathbf{V} \in \mathcal{U}(K)$ in (40).

When $K > M$, the integral $\mathcal{J}_2(\mathbf{\Omega}) = \int_{\mathcal{U}(K)} \exp(-\mathrm{tr}\mathbf{V}\mathbf{\Omega}\mathbf{V}^\dagger\mathbf{\Sigma}^{-1})d\mathbf{V}$ is obtained by applying Lemma 1 to (37) when taking the limit $\omega_{M+1}, \dots, \omega_K \to 0$. That is,

$$\mathcal{J}_2(\mathbf{\Omega}) = \left(\prod_{j=K-M}^{K-1}\Gamma(j+1)\right)\frac{(\det\mathbf{\Sigma})^{K-1}}{\Delta_M(\boldsymbol{\omega})\Delta_K(\boldsymbol{\sigma})\prod_{i=1}^M \omega_i^{K-M}}\det\left[\begin{array}{c}\{(-\sigma_j)^{1-i}\}_{\substack{1 \leq i \leq K-M \\ 1 \leq j \leq K}} \\ \{\exp(-\omega_i/\sigma_j)\}_{\substack{1 \leq i \leq M \\ 1 \leq j \leq K}}\end{array}\right].$$

The denominator of (40) is solved by (38) by interchanging K and M. Then, after inserting $\mathcal{J}_1(\mathbf{\Omega})$ and $\mathcal{J}_2(\mathbf{\Omega})$ into (40), we obtain $\phi(s)$ for $K > M \geq n$ as

$$\phi(s) = \frac{1}{M!}\frac{(\det\mathbf{\Sigma})^{K-M-1}}{\prod_{j=1}^{M-1}\Gamma(j+1)}\frac{\prod_{j=1}^n \gamma_j^{n-M}}{\Delta_n(\boldsymbol{\gamma})\Delta_K(\boldsymbol{\sigma})}\prod_{j=K-n}^{K-1}\frac{\Gamma(s+K-j)\Gamma(j+1)}{\Gamma(s+M)\Gamma(K-M+1)}$$

$$\times \int_{[0,\infty)^M}\det\left[\begin{array}{c}\{\omega_j^{i-1}\}_{\substack{1 \leq i \leq M-n \\ 1 \leq j \leq M}} \\ \left\{{}_2F_1\binom{1,1-s-M}{K-M+1}\Big|-\omega_j\gamma_i\right\}_{\substack{1 \leq i \leq n \\ 1 \leq j \leq M}}\end{array}\right]\det\left[\begin{array}{c}\{(-\sigma_j)^{1-i}\}_{\substack{1 \leq i \leq K-M \\ 1 \leq j \leq K}} \\ \left\{\exp\left(-\frac{\omega_i}{\sigma_j}\right)\right\}_{\substack{1 \leq i \leq M \\ 1 \leq j \leq K}}\end{array}\right]d\boldsymbol{\omega}$$

$$= \frac{\prod_{j=1}^n \gamma_j^{n-M}}{\Delta_n(\boldsymbol{\gamma})\Delta_K(\boldsymbol{\sigma})}\prod_{j=K-n}^{K-1}\frac{\Gamma(s+K-j)\Gamma(j+1)}{\Gamma(j-K+M+1)\Gamma(s+M)\Gamma(K-M+1)}$$

$$\times \det\left[\{\sigma_i^{j-1}\}_{\substack{1 \leq i \leq K \\ 1 \leq j \leq K-n}} \quad \left\{\sigma_j^{K-M}\,{}_3F_1\binom{1,1,1-s-M}{K-M+1}\Big|-\sigma_j\gamma_i\right\}_{\substack{1 \leq i \leq K \\ 1 \leq j \leq n}}\right], \quad (43)$$

where the second equality is obtained by applying Lemma 2 and the identity [37, Eq. (7.811.1)].

When $K > n > M$, we obtain $\phi(s)$ as

$$\phi(s) = \frac{1}{M!} \frac{(\det \boldsymbol{\Sigma})^{K-M-1}}{\Delta_n(\boldsymbol{\gamma})\Delta_K(\boldsymbol{\sigma})\prod_{j=0}^{M-1}\Gamma(j+1)} \prod_{j=n-M}^{n-1} \frac{\Gamma(s+n-j)\Gamma(j+K-n+1)}{\Gamma(s+M)\Gamma(K-M+1)}$$

$$\times \int_{[0,\infty)^M} \det \begin{bmatrix} \left\{\gamma_j^{i-1}\right\}_{\substack{1\leq i\leq n-M \\ 1\leq j\leq n}} \\ \left\{\gamma_j^{n-M} \, {}_2F_1\left(\begin{matrix}1,1-s-M \\ K-M+1\end{matrix}\middle| -\omega_i\gamma_j\right)\right\}_{\substack{1\leq i\leq M \\ 1\leq j\leq n}} \end{bmatrix} \det \begin{bmatrix} \left\{(-\sigma_j)^{1-i}\right\}_{\substack{1\leq i\leq K-M \\ 1\leq j\leq K}} \\ \left\{\exp\left(-\frac{\omega_i}{\sigma_j}\right)\right\}_{\substack{1\leq i\leq M \\ 1\leq j\leq K}} \end{bmatrix} d\boldsymbol{\omega}$$

$$= \frac{(-1)^{(K-M)(n-M)}}{\Delta_n(\boldsymbol{\gamma})\Delta_K(\boldsymbol{\sigma})} \prod_{j=n-M}^{n-1} \frac{\Gamma(s+n-j)\Gamma(j+K-n+1)}{\Gamma(j+M-n+1)\Gamma(s+M)\Gamma(K-M+1)}$$

$$\times \det \begin{bmatrix} \left\{0\right\}_{\substack{1\leq i\leq K-M \\ 1\leq j\leq n-M}} & \left\{\sigma_j^{i-1}\right\}_{\substack{1\leq i\leq K-M \\ 1\leq j\leq K}} \\ \left\{\gamma_i^{j-1}\right\}_{\substack{1\leq i\leq n \\ 1\leq j\leq n-M}} & \left\{\gamma_i^{n-M}\sigma_j^{K-M} \, {}_3F_1\left(\begin{matrix}1,1,1-s-M \\ K-M+1\end{matrix}\middle| -\sigma_j\gamma_i\right)\right\}_{\substack{1\leq i\leq n \\ 1\leq j\leq K}} \end{bmatrix},$$

where we applied Lemma 2 in the second equality.

REFERENCES

[1]   Y. Liang, H. V. Poor, and S. Shamai, *Information Theoretic Security*. Delft, The Netherlands: Now Publishers, 2009.

[2]   A. D. Wyner, "The wire-tap channel," *Bell Syst. Tech. J.*, vol. 54, no. 8, pp. 1355–1387, Oct. 1975.

[3]   I. Csiszar and J. Korner, "Broadcast channels with confidential messages," *IEEE Trans. Inf. Theory*, vol. 24, no. 3, pp. 339–348, May 1978.

[4]   P. K. Gopala, L. Lai, and H. E. Gamal, "On the secrecy capacity of fading channels," *IEEE Trans. Inf. Theory*, vol. 54, no. 10, pp. 4687–4698, Oct. 2008.

[5]   A. O. Hero, "Secure space-time communication," *IEEE Trans. Inf. Theory*, vol. 49, no. 12, pp. 3235–3249, Dec. 2003.

[6]   P. Parada and R. Blahut, "Secrecy capacity of SIMO and slow fading channels," in *Proc. IEEE Int. Symp. Inf. Theory,* Adelaide, Australia, Sept. 2005, pp. 2152–2155.

[7]   J. Zhu, Y. Zou, G. Wang, Y. D. Yao, and G. K. Karagiannidis, "On secrecy performance of antenna-selection-aided MIMO systems against eavesdropping," *IEEE Trans. Veh. Technol.*, vol. 65, no. 1, pp. 214–225, Jan. 2016.

[8]   Z. Li, W. Trappe, and R. Yates, "Secret communication via multi-antenna transmission," in *Proc. 41st Conf. Information Sciences Systems*, Baltimore, MD, Mar. 2007, pp. 905–910.

[9]   S. Shafiee and S. Ulukus, "Achievable rates in Gaussian MISO channels with secrecy constraints," in *Proc. IEEE Int. Symp. Inf. Theory*, Nice, France, June 2007, pp. 2466–2470.

[10]   S. Shafiee, N. Liu, and S. Ulukus, "Towards the secrecy capacity of the Gaussian MIMO wire-tap channel: The 2-2-1 channel," *IEEE Trans. Inf. Theory*, vol. 55, no. 9, pp. 4033–4039, Sept. 2009.

[11]   D. W. K. Ng and R. Schober, "Secure and green SWIPT in distributed antenna networks with limited backhaul capacity," *IEEE Trans. Wireless Commun.*, vol. 14, no. 9, pp. 5082–5097, Sept. 2015.

[12]   H. M. Wang, C. Wang, D. W. K. Ng, M. H. Lee, and J. Xiao, "Artificial noise assisted secure transmission for distributed antenna systems," *IEEE Trans. Signal Process.*, vol. 64, no. 15, pp. 4050–4064, Aug. 2016.

[13]   H. Jin and J. Kim, "Combined antenna selection and beamforming for secure transmission in distributed antenna systems,"

in *Proc. Int. Conf. ICT Convergence*, Jeju, South Korea, Oct. 2013, pp. 1043–1047.

[14] C. Wang and Z. Wang, "Signal alignment for secure underwater coordinated multipoint transmissions," *IEEE Trans. Signal Process.*, vol. 64, no. 23, pp. 6360–6374, Dec. 2016.

[15] M. Zhang, R. Xue, H. Yu, H. Luo, and W. Chen, "Secrecy capacity optimization in coordinated multi-point processing," in *Proc. 2013 IEEE Int. Conf. Commun.*, Budapest, Hungary, June 2013, pp. 5845–5849.

[16] A. Abdi and M. Kaveh, "A space-time correlation model for multielement antenna systems in mobile fading channels," *IEEE J. Sel. Areas Commun.*, vol. 20, no. 3, pp. 550–560, Apr. 2002.

[17] D. Gesbert, H. Bolcskei, D. A. GORE, and A. J. Paulraj, "Outdoor MIMO wireless channels: models and performance prediction," *IEEE Trans. Commun.*, vol. 50, no. 12, pp. 1926–1934, Dec. 2002.

[18] A. Khisti and G. W. Wornell, "Secure transmission with multiple antennas I: The MISOME wiretap channel," *IEEE Trans. Inf. Theory*, vol. 56, no. 7, pp. 3088–3104, July 2010.

[19] F. Oggier and B. Hassibi, "The secrecy capacity of the MIMO wiretap channel," *IEEE Trans. Inf. Theory*, vol. 57, no. 8, pp. 4961–4972, Aug. 2011.

[20] A. Khisti and G. W. Wornell, "Secure transmission with multiple antennas part II: The MIMOME wiretap channel," *IEEE Trans. Inf. Theory*, vol. 56, no. 11, pp. 5515–5532, Nov. 2010.

[21] R. Bustin, R. Liu, H. V. Poor, and S. Shamai, "An MMSE approach to the secrecy capacity of the MIMO Gaussian wiretap channel," *EURASIP J. Wireless Commun. Netw.*, vol. 2009, no. 1, p. 370970, July 2009.

[22] S. A. A. Fakoorian and A. L. Swindlehurst, "Full rank solutions for the MIMO Gaussian wiretap channel with an average power constraint," *IEEE Trans. Signal Process.*, vol. 61, no. 10, pp. 2620–2631, May 2013.

[23] S. Loyka and C. D. Charalambous, "Optimal signaling for secure communications over Gaussian MIMO wiretap channels," *IEEE Trans. Inf. Theory*, vol. 62, no. 12, pp. 7207–7215, Dec. 2016.

[24] J. Li and A. P. Petropulu, "On ergodic secrecy rate for Gaussian MISO wiretap channels," *IEEE Trans. Wireless Commun.*, vol. 10, no. 4, pp. 1176–1187, Apr. 2011.

[25] P. H. Lin, S. H. Lai, S. C. Lin, and H. J. Su, "On secrecy rate of the generalized artificial-noise assisted secure beamforming for wiretap channels," *IEEE J. Sel. Areas Commun.*, vol. 31, no. 9, pp. 1728–1740, Sept. 2013.

[26] J. Li and A. P. Petropulu, "Ergodic secrecy rate for multiple-antenna wiretap channels with Rician fading," *IEEE Trans. Inf. Forensics Security*, vol. 6, no. 3, pp. 861–867, Sept. 2011.

[27] T. V. Nguyen and H. Shin, "Power allocation and achievable secrecy rates in MISOME wiretap channels," *IEEE Commun. Lett.*, vol. 15, no. 11, pp. 1196–1198, Nov. 2011.

[28] S. C. Lin and C. L. Lin, "On secrecy capacity of fast fading MIMOME wiretap channels with statistical CSIT," *IEEE Trans. Wireless Commun.*, vol. 13, no. 6, pp. 3293–3306, June 2014.

[29] S. Vishwakarma and A. Chockalingam, "Power allocation in MIMO wiretap channel with statistical CSI and finite-alphabet input," in *Proc. 2014 Int. Conf. Signal Process. Commun.*, Bangalore, India, July 2014.

[30] Y. Wu, C. Xiao, Z. Ding, X. Gao, and S. Jin, "Linear precoding for finite-alphabet signaling over MIMOME wiretap channels," *IEEE Trans. Veh. Technol.*, vol. 61, no. 6, pp. 2599–2612, July 2012.

[31] A. Zappone, P. H. Lin, and E. A. Jorswieck, "Secrecy and energy efficiency in MIMO-ME systems," in *Proc. 16th IEEE Int. Workshop Signal Process. Advances in Wireless Commun.*, Stockholm, Sweden, June 2015, pp. 380–384.

[32] Z. Zheng and Z. J. Haas, "On the performance of reconfigurable distributed MIMO in mobile networks," *IEEE Trans. Commun.*, vol. 65, no. 4, pp. 1609–1622, Apr. 2017.

[33] M. R. Bloch and J. N. Laneman, "Strong secrecy from channel resolvability," *IEEE Trans. Inf. Theory*, vol. 59, no. 12, pp.

8077–8098, Dec. 2013.

[34] E. Telatar, "Capacity of multi-antenna Gaussian channels," *Eur. Trans. Telecommun.*, vol. 10, no. 6, pp. 585–595, 1999.

[35] Y. Zhu, Y. Zhou, S. Patel, X. Chen, L. Pang, and Z. Xue, "Artificial noise generated in MIMO scenario: Optimal power design," *IEEE Signal Process. Lett.*, vol. 20, no. 10, pp. 964–967, Oct. 2013.

[36] S. H. Simon, A. L. Moustakas, and L. Marinelli, "Capacity and character expansions: Moment-generating function and other exact results for MIMO correlated channels," *IEEE Trans. Inf. Theory*, vol. 52, no. 12, pp. 5336–5351, Dec. 2006.

[37] S. Sternberg, *Group Theory and Physics*. Cambridge University Press, 1995.

[38] I. S. Gradshteyn and I. M. Ryzhik, *Table of integrals, series, and products*. Academic press, 2014.

[39] J. R. Magnus and H. Neudecker, *Matrix Differential Calculus with Applications in Statistics and Econometrics*. Wiley, 1999.

[40] F. W. J. Olver, D. W. Lozier, R. F. Boisvert, and C. W. Clark, Eds., *NIST Handbook of Mathematical Functions*, 1st edition. Cambridge; New York: Cambridge University Press, 2010.

[41] M. Grant and S. Boyd, "CVX: Matlab software for disciplined convex programming, ver. 2.0 beta." [Online]. Available: http://cvxr.com/cvx/.

[42] M. C. Grant and S. P. Boyd, "Graph implementations for nonsmooth convex programs," in *Recent Advances in Learning and Control*, Springer, London, 2008, pp. 95–110.

[43] K. Cumanan, Z. Ding, B. Sharif, G. Y. Tian, and K. K. Leung, "Secrecy rate optimizations for a MIMO secrecy channel with a multiple-antenna eavesdropper," *IEEE Trans. Veh. Technol.*, vol. 63, no. 4, pp. 1678–1690, May 2014.

[44] M. Kieburg and T. Guhr, "Derivation of determinantal structures for random matrix ensembles in a new way," *J. Phys. Math. Theor.*, vol. 43, no. 7, p. 075201, 2010.

[45] A. M. Mathai, *Jacobians of Matrix Transformations and Functions of Matrix Arguments*. World Scientific Publishing Co Inc, 1997.

[46] K. I. Gross and D. S. P. Richards, "Total positivity, spherical series, and hypergeometric functions of matrix argument," *J. Approx. Theory*, vol. 59, no. 2, pp. 224–246, Nov. 1989.

[47] C. Itzykson and J. B. Zuber, "The planar approximation. II," *J. Math. Phys.*, vol. 21, no. 3, pp. 411–421, 1980.

[48] M. L. Mehta, *Random Matrices*. Academic Press, 2004.